

A SOIL IMPROVEMENT CASE STUDY USING RAMMED STONE COLUMN SYSTEMS

A THESIS SUBMITTED TO  
THE GRADUATE SCHOOL OF NATURAL AND APPLIED SCIENCES  
OF  
MIDDLE EAST TECHNICAL UNIVERSITY

BY

OSMAN FATİH BEŞLER

IN PARTIAL FULFILLMENT OF THE REQUIREMENTS  
FOR  
THE DEGREE OF THE MASTER OF SCIENCE  
IN  
CIVIL ENGINEERING

MAY 2013



Approval of the thesis:

**A SOIL IMPROVEMENT CASE STUDY USING RAMMED STONE COLUMN  
SYSTEMS**

submitted by **OSMAN FATİH BEŞLER** in partial fulfillment of the requirements for the degree  
of **Master of Science in Civil Engineering Department, Middle East Technical University**  
by,

Prof. Dr. Canan Özgen  
Dean, Graduate School of **Natural and Applied Science** \_\_\_\_\_

Prof. Dr. Ahmet Cevdet Yalçiner  
Head of Department, **Civil Engineering** \_\_\_\_\_

Prof. Dr. Bahadır Sadık Bakır  
Supervisor, **Civil Engineering Dept., METU** \_\_\_\_\_

**Examining Committee Members:**

Prof. Dr. Erdal Çokça  
Civil Engineering Dept., METU \_\_\_\_\_

Prof. Dr. Bahadır Sadık Bakır  
Civil Engineering Dept., METU \_\_\_\_\_

Prof. Dr. Tamer Topal  
Geological Engineering Dept., METU \_\_\_\_\_

Asst. Prof. Dr. Nejan Huvaj Sarihan  
Civil Engineering Dept., METU \_\_\_\_\_

Onur Başer  
Civil Engineering Ms. Sc. \_\_\_\_\_

**Date:** 31/05/2013

**I hereby declare that all information in this document has been obtained and presented in accordance with academic rules and ethical conduct. I also declare that, as required by these rules and conduct, I have fully cited and referenced all material and results that are not original to this work.**

Name, Last name : Osman Fatih Beşler

Signature :

## ABSTRACT

### A SOIL IMPROVEMENT CASE STUDY USING RAMMED STONE COLUMN SYSTEM

Beşler, Osman Fatih  
M.Sc., Department of Civil Engineering  
Supervisor: Prof Dr. B. Sadık Bakır

May, 2013, 72 pages

Nowadays, the rammed stone columns and similar systems are used worldwide more and more frequently as an economical way for improvement of the foundation soils. The primary objective of this study is to evaluate the effectiveness of the rammed stone column system by predicting settlements and bearing capacity increase through evaluation of failure mechanisms of reinforced soil layers loaded in compression. Conventional approaches of design are compared with the results of finite element models using software PLAXIS 3D and field load test. Field and laboratory tests are carried out to determine the attributes of the in-situ foundation soils .

It is found that the predictive capability of available methods for the evaluation of bearing capacity of the reinforced soil fits well with that derived from field load tests, in general. Response of a single loaded column and group of loaded columns don't show significant differences. On the other hand, regarding elastic settlements some differences were observed between the field test results and those calculated from the finite element model, as well as those estimated by the existing formulations. Potential reasons for those differences are discussed in this thesis.

**Keywords:** Bearing capacity, finite element model, load-settlement curve, plate load test, PLAXIS 3D, rammed stone column, settlement, soil improvement methods, stone column,

## ÖZ

### DARBEYLE SIKIŞTIRILMIŞ TAŞ KOLON KULLANILARAK YAPILAN BİR ZEMİN İYİLEŞTİRME VAKA ANALİZİ

Beşler, Osman Fatih  
Yüksek Lisans, İnşaat Mühendisliği Bölümü  
Tez Yöneticisi: Prof. Dr. B. Sadık Bakır

Mayıs 2013, 72 sayfa

Günümüzde, temel zeminini iyileştirmek için darbeyle sıkıştırılmış taş kolon ve benzer sistemler dünya çapında ekonomik bir yöntem olarak gittikçe daha sık kullanılmaktadır.

Bu çalışmanın temel amacı, iyileştirilmiş zemin tabakalarının basınç altında oturma miktarlarını ve göçme mekanizmalarına bağlı taşıma kapasitesi artışını tahmin ederek, darbeyle sıkıştırılmış taş kolon yönteminin verimliliğini değerlendirmektir. Klasik tasarım yaklaşımları, sonlu elemanlar programı PLAXİS 3D ve arazi yükleme sonuçları ile karşılaştırılmıştır. Temel zemininin belirleyici özelliklerini tanımlayabilmek için saha ve laboratuvar deneyleri gerçekleştirilmiştir.

İyileştirilmiş zeminin taşıma kapasitesi için mevcut yöntemlerden tahmin edilen kapasite, arazi yükleme deneylerinden elde edilen sonuçlar ile genel olarak benzerlik göstermektedir. Tek kolon üzerinde yapılan yükleme deney ve çoklu grup üzerinde yapılan yükleme deney sonuçları önemli farklılık göstermemektedir. Diğer taraftan, sonlu elemanlar yöntemi kullanılarak hesaplanan ve aynı şekilde mevcut formüllerden tahmin edilen elastik oturma miktarları saha ölçümlerinden farklılıklar göstermektedir. Bu farklılıklar için potansiyel nedenler bu tezde tartışılmıştır.

**Anahtar Kelimeler:** Taşıma kapasitesi, sonlu elemanlar modeli, yük-deplasman grafiği, plaka yükleme deneyi, PLAXIS 3D, darbeyle sıkıştırılmış taş kolon, oturma, zemin iyileştirme yöntemleri, taş kolon

*To My Family*

## ACKNOWLEDGEMENTS

I would like to present my sincere gratitude to Prof. Dr. Bahadır Sadık BAKIR for his valuable guidance, encouragement and insight throughout this study. In addition, I express my deepest appreciation to him for his useful advices enlightening my understanding of the engineering.

I would like to thank Mr. Osman AYDOĞDU not only for the financial support during this study, but also for his encouragements and providing of motivation.

Certainly, İKSA Co. Employees are gratefully acknowledged for their emotional support during this study.

I am thankful to all my friends who shared the difficult and happy moments of this adventure.

I would also like to thank to all of the Limit Co. Members who provided technical support regarding the laboratory work.

Finally yet importantly, I should certainly thank to my parents for their incredible patience with me, for their endless belief in me during the hard working periods of this study.

## TABLE OF CONTENTS

ABSTRACT.....	v
ÖZ.....	vi
ACKNOWLEDGEMENTS.....	viii
TABLE OF CONTENTS.....	ix
LIST OF TABLES.....	xi
LIST OF FIGURES.....	xii
CHAPTERS.....	1
1. INTRODUCTION.....	1
2. LITERATURE REVIEW.....	3
2.1 A general look at the development of rammed stone columns.....	3
2.2 Ultimate bearing capacity analysis of footing bearing on soils reinforced with rammed stone columns.....	6
2.2.1 Bearing capacity of soil reinforced with a single rammed stone column.....	6
2.2.2 Bearing capacity of soil reinforced with a rammed stone column group.....	13
2.3 Settlement calculations of footings on soil reinforced with rammed stone columns.....	16
2.3.1 Evaluation of the stress concentration ratio.....	18
2.3.2 Immediate settlement of the upper zone.....	19
2.3.3 Immediate and consolidation settlement of the lower zone.....	22
2.4 Strength parameters of rammed stone column material.....	23
2.4.1 Shear strength of construction material.....	23
2.4.2 Modulus of subgrade reaction for single rammed stone column.....	24
2.5 Determination of ultimate bearing capacity from stress-settlement data.....	26
2.5.1 Chin-Kondner method.....	27
2.5.2 Mazurkiewicz's method.....	27
2.5.3 Decourt's extrapolation method.....	28
2.6 Classical methods for the bearing capacity calculation.....	29
3. EXPERIMENTAL AND NUMERICAL STUDY.....	31
3.1 Classification and engineering properties of the site soils.....	32
3.2 Construction of the rammed stone columns.....	33
3.3 Determination of the engineering properties of rammed stone columns.....	34
3.3.1 Sieve analysis.....	34
3.3.2 Evaluation of modulus of subgrade reaction for single rammed stone column.....	35
3.4 Bearing capacity calculations of reinforced soil.....	38
3.4.1 Bulging failure of individual rammed stone columns.....	39

3.4.2	Shearing failure below tips of individual rammed stone columns.....	40
3.4.3	Shearing failure within the reinforced soil zone.....	41
3.4.4	Shearing failure below the reinforced soil zone .....	42
3.5	Settlement calculations of reinforced soil .....	43
3.5.1	Immediate settlement of the upper zone.....	44
3.5.2	Immediate settlement of the lower zone.....	44
3.6	Plate load test on a group of rammed stone columns .....	45
3.6.1	Determination of ultimate bearing capacity from stress-settlement data.....	47
3.6.2	Comparison of settlements from single and group rammed stone column tests.....	47
3.7	Evaluation of the reinforced model using finite element method .....	48
3.7.1	General model properties .....	49
3.7.2	Material properties .....	49
3.7.3	Analyses of the model .....	50
3.7.4	Analyses results.....	51
4.	SUMMARY, DISCUSSIONS AND CONCLUSIONS .....	53
4.1	Summary .....	53
4.2	Discussions and conclusions .....	53
	REFERENCES .....	55
	LIST OF NOTATIONS USED IN THE TEXT .....	58

## LIST OF TABLES

### TABLES

Table 2.1 Observed stress concentration ratios on stone columns (Barksdale and Bachus, 1983).....	19
Table 2.2 Typical Geopier design parameter for peat and organic foundation soils (Fox and Cowell, 1998).....	25
Table 3.1 Properties of the site soils.....	33
Table 3.2 Sieve analysis results of the rammed stone column material .....	35
Table 3.3 Settlement records from the load test of a single column.....	36
Table 3.4 Rammed stone column parameters.....	38
Table 3.5 Dimensions of the group plate load test setup.....	39
Table 3.6 Failure mechanism and respective bearing capacity of the reinforced soil .....	43
Table 3.7 Elastic settlement calculations .....	45
Table 3.8 Settlement records of the group load test .....	46
Table 3.9 Settlement readings from loading-unloading curve of the plate load test on group of columns .....	47
Table 3.10 Comparison of ultimate bearing capacity results of different methods .....	47
Table 3.11 Comparison of settlement readings of single loaded column and group of columns	48

## LIST OF FIGURES

### FIGURES

Figure 2.1 Typical construction process for vibro-compaction (Green, 2001) .....	3
Figure 2.2 Installation method of stone column using dry method (Hayward Baker Inc., 1996) .....	4
Figure 2.3 Typical construction process of Geopier (a) Creating creating cavity (b) Making the bottom bulb (c) Building shaft with undulating layers (d) Installation complete (Gaul, 2001) .....	5
Figure 2.4 Failure mechanisms for single pier in homogeneous soil: (a) Bulging, (b) General or local shear (c) Punching (Barksdale and Bachus, 1983) .....	6
Figure 2.5 Deformation of stone column (Hughes and Withers, 1974) .....	7
Figure 2.6 Expansion of cylindrical cavity (Vesic, 1972).....	9
Figure 2.7 Cavity expansion factors (Vesic, 1972).....	9
Figure 2.8 Possible failure mechanisms in Geopier groups: (a) Local shear within pier-reinforced matrix zone; (b) Individual punching; and (c) Shearing below pier-reinforced matrix zone (Fox and Cowell, 1998) .....	13
Figure 2.9 Idealization of unit cell: (a) Plan view (b) Unit cell (c) Vertical cross section (modified from Barksdale and Bachus, 1983).....	15
Figure 2.10 Upper zone and lower zone beneath an isolated footing (from Fox and Cowell, 1998)....	17
Figure 2.11 Spring analogy for stress concentration along interface of footing and Geopier-reinforced bearing soil (modified from Fox and Cowell, 1998) .....	20
Figure 2.12 Factors to be used for the calculation of elastic settlement (Christian and Carrier, 1978).23	
Figure 2.13 Results obtained from full-scale direct shear tests performed on Geopier elements (modified from Fox and Cowell, 1998).....	23
Figure 2.14 Small-scale laboratory triaxial tests results on reconstituted samples of well-graded Geopier aggregate compacted to densities consistent with those measured for installed Geopier elements (White, 2001) .....	24
Figure 2.15 Plate load test setup (Bowles, 1996).....	25
Figure 2.16 Determination of ultimate bearing stress from settlement data: (a) Footing showing nomenclature, (b) Sample load-settlement curves (modified from Vesic, 1975) .....	26
Figure 2.17 Load-settlement curve of an axial loaded continuous flight auger pile (Abdelrahman, et al., 2003).....	27
Figure 2.18 Estimation of ultimate failure load according to Mazurkiewicz (Abdelrahman et al., 2003) .....	28
Figure 2.19 Estimation of ultimate failure load according to Decourt's extrapolation method (Abdelrahman et al., 2003) .....	29
Figure 3.1 Conducted plate load test setup on reinforced soil .....	31
Figure 3.2 Construction of the rammed stone columns at field.....	33
Figure 3.3 Tamper at the tip of the drill rig.....	34
Figure 3.4 Grain size distribution of the aggregate used for the construction of the columns .....	35
Figure 3.5 Set up of the single rammed stone column test.....	36
Figure 3.6 Induced stress versus measured settlement from single column load test .....	37
Figure 3.7 A view of the group load test setup .....	45
Figure 3.8 Load-settlement plot recorded during group load test .....	46
Figure 3.9 Comparison of the stress-displacement plots of a single loaded column and group columns .....	48
Figure 3.10 (a) Input geometry of the analyzed model in PLAXIS 3D (b) Generated mesh .....	49
Figure 3.11 Cross section showing settlements at maximum stress step .....	51
Figure 3.12 Comparison of stress-settlement responses.....	52





## CHAPTER 1

### INTRODUCTION

The high costs forced geotechnical engineers to search for economical alternative solutions basically including the improvement of foundation soils through various techniques. Soil improvement methods include excavation and replacement, deep dynamic compaction, sand and stone columns, grouting and chemical stabilization, as well as many others. The selection of these methods depends on the demand whether to increase the shear strength of soil; reduce or increase the permeability of soil in order to limit the water flow or accelerate settlements or improvement of homogeneity in order to equalize deformation.

Except the method of replacement, ground improvement methods can be divided into subheadings like compaction (dynamic methods) and reinforcement methods such as vibro stone columns, vibro concrete columns, grouting etc. There exist several types of construction of stone columns such as vibro-replacement (wet) method, vibro-displacement method or rammed stone columns depending on the soil conditions or the preference of the designer.

This study focuses on the investigation of performance of rammed stone columns. The method is applied by driving a closed end pipe into the ground by vertical vibration until required depth is reached. After crushed stone is poured from top of the pipe, the pipe is raised about 1 meter. While raising the pipe, the shutting at the bottom of the pipe is opened by gravity and crushed stone is cast into the driven hole. Afterwards, the pipe is pushed downwards by vertical vibration about 60 cm which compresses the crushed stone inside the hole and forces it to spread horizontally into the surrounding soil. This process is repeated until the desired length of the column is formed. The main goal in this method is to densify the crushed stone in the hole as well as the surrounding soil.

Similar methods with minor differences which aim the same purpose exist as that of rammed stone columns, and a number of these have been patented. Numerous research studies have been undertaken in order to provide a better understanding of how reinforced soils respond to applied loads, and to establish design principles of such systems.

The work described in this thesis is intended to be an examination of the existing practice regarding design and implementation. More specifically, the scope of the study is to evaluate existing design principles for the rammed stone columns with actual obtained values from plate load tests and finite element methods. The following works have been carried out for that purpose:

- ✓ Existing design principles for bearing capacity and settlement prediction for a footing loaded in compression and supported by rammed stone columns are evaluated. Results of field compression load tests at a specific site are compared with those.
- ✓ Response of a group of closely spaced rammed stone columns subjected to compressive load are compared with that of a single rammed stone column loaded in compression in the same soil formation with equivalent diameter and length.

In order to achieve the above stated objectives, several tasks have been fulfilled before and after the application of the rammed stone columns. These are:

- ✓ Standard penetration and pressuremeter tests were conducted before construction. Results from these tests were used to determine the relevant engineering properties of the foundation soils.

- ✓ Laboratory tests were conducted on disturbed and undisturbed soil specimens in accordance with the following specifications:
  - Water content (TS 1900-1)
  - Atterberg limits (TS 1900-1)
  - Sieve analysis (ASTM 2487/90)
  - Unit weight (TS 1900-1)
  - Triaxial compression test - UU (TS 1900-2)
  - Soil classification (ASTM D 2487-11)
  - Direct shear test (ASTM D3080/D3080M)
- ✓ In order to evaluate the response of a rammed stone column for the estimation of stiffness and modulus of elasticity, a single column has been loaded under compression.
- ✓ In order to compare the results of empirical calculations regarding settlement, bearing capacity and group effect of the rammed stone columns to those of a single column, a cap is constructed on a group of the rammed stone column reinforced soil, and is loaded under compression. Test data were gathered and analyzed. The load test was conducted according to ASTM D 1143-81 Standards.
- ✓ Field load tests with a group of the rammed stone column elements were simulated through finite element models using PLAXIS 3D software, and findings were compared with those of measured and calculated using empirical formulas.

## CHAPTER 2

### LITERATURE REVIEW

#### 2.1 A general look at the development of rammed stone columns

Before rammed stone column technique was specifically developed, stone columns were utilized as an effective soil improvement method. A system, which is called vibro-compaction or vibroflotation, was enhanced in order to improve weak soil layers (Brown and Glenn, 1976; Brown, 1977; Saito, 1977; Lopez and Hayden, 1992). The construction process, as shown in Figure 2.1, consists of forming a cavity in the ground using vibrator until the required depth is reached and by raising and lowering the vibrator and backfilling. The backfill material used for this technique is typically sand.

The stone column technique is actually similar to the vibro-compaction method (Figure 2.1) with the difference that generally gravel or crushed stone is used as backfill. Stone columns can be installed in dry or wet method (Munfakh et al., 1987; Hayward Baker Inc., 1996) depending on the conditions. In order to ease the advance of the vibrator in the dry method (Figure 2.2), compressed air is used. This method is called vibro-displacement stone columns.

The bottom feed technique has its name from the method of pouring crushed stone or gravel in to the hole. It is fed by pipes directly to the nose of the vibrator. In the top feed method, the stone is fed to the annulus circular ring of the vibrator, which falls by gravity and vibrations through the bottom of the annulus ring to the created hole.

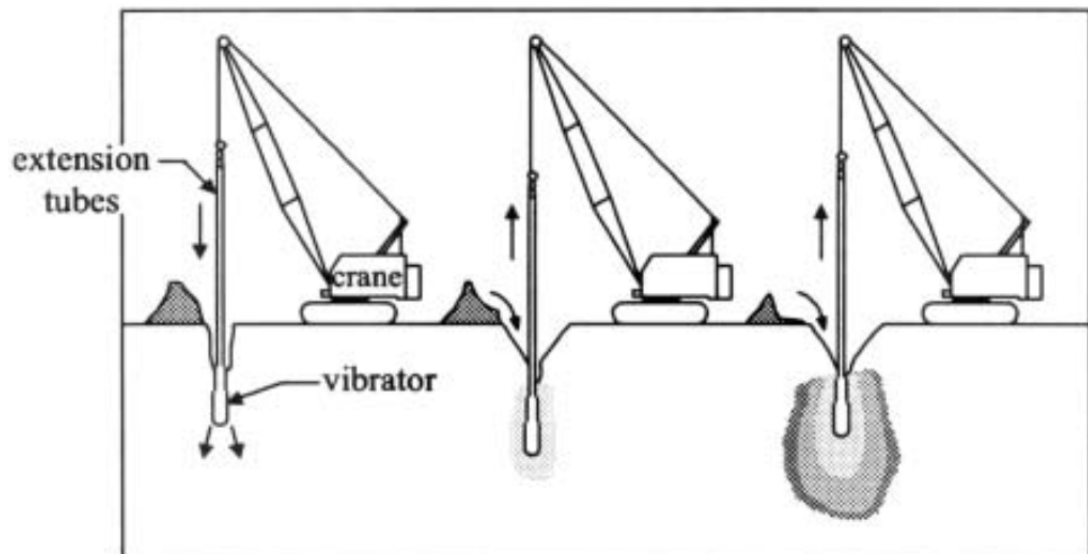


Figure 2.1 Typical construction process for vibro-compaction (Green, 2001)

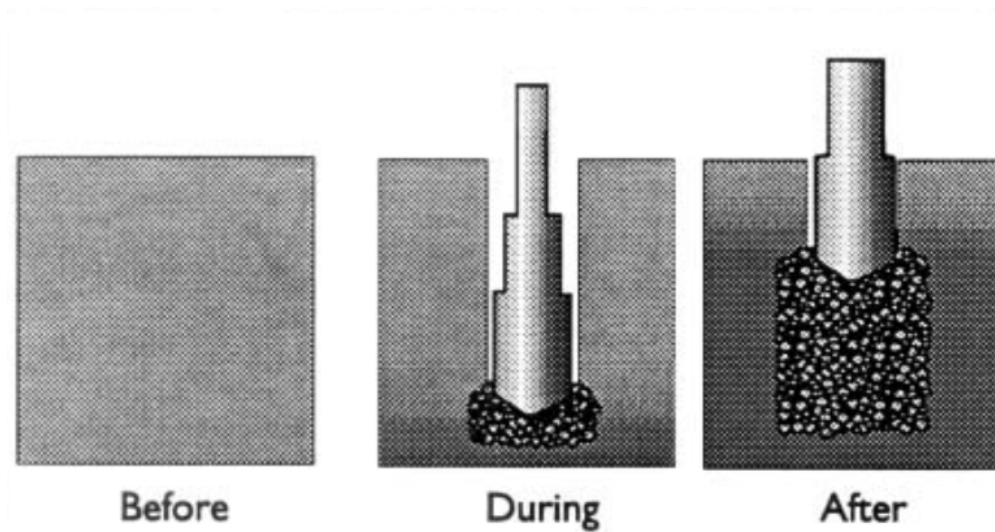


Figure 2.2 Installation method of stone column using dry method (Hayward Baker Inc., 1996)

The vibratory probe method uses heavy vibrator that is clamped to the upper end of a long steel probe. The difference of the vibratory probe method from classical stone columns is that it induces vertical vibrations. Typical construction process includes the advance of the probe to the desired depth and densification of the soil during extraction of the probe. Backfill material is not commonly used for this method (Russell, 2001).

In the last twenty five years an alternative solution which is a special way of stone column has been used widely in order to improve weak soil conditions. The method, which is called “rammed stone column”, is especially beneficial in cohesive soils and consists of compacted stone columns. The rammed stone column is constructed by driving the casing until required depth is reached, usually by hammering on a temporary stone or sand plug located at the bottom of the casing. The height of fall, usually 4-6 m, is chosen considering the soil strength and project requirements. When the specified depth is reached, the plug is driven out by hammering with the casing maintained in position or slightly pulled up by tension ropes (Barksdale and Bachus, 1983). Rammed stone columns are constructed by either driving an open or closed end pipe in the ground or boring a hole. Sand or stone is placed in the hole in increments, and in using a heavy, falling weight (FHWA Reports, 1983).

A similar system, which is known as Geopier system with a special designed rammer awarded a U.S. patent (Fox and Lawton, 1993) owing to its uniqueness. The installation procedure is defined by Fox and Cowell (1998) as shown in Figure 2.3. A hole is excavated with the use of a drill rig. “clean stone” (crushed stone without fines, max. diameter 50 mm or 2 in) is placed into the hole. A high frequency, impact tamper with a specially designed 45-degree beveled head is used to compact the aggregate, which results in increased vertical and horizontal stresses in the adjacent matrix soil during and after impact. During this process, the diameter of the pier is increased by approximately 76 mm (3 in.) beyond the nominal dimensions of the hole. In addition, an estimated one-pier diameter increase in length occurs owing to the creation of a bulb at the bottom of the pier. This increase in the size of the pier pre-stresses and pre-strains the adjacent soil. An undulated-sided pier shaft is formed continuously up to the basement level by the same ramming action. During densification of the crushed stone, stone is also forced to move laterally, thus increasing lateral stress of the surrounding soil which tends to increase stiffness of the composite pier-soil system. This also increases bearing capacity of the reinforced zone and reduces settlements. There are several types of Geopier systems

which differ through the type of installation such as the Armorpact system, GP3 System, Impact system, Rampact system and Densipact system.

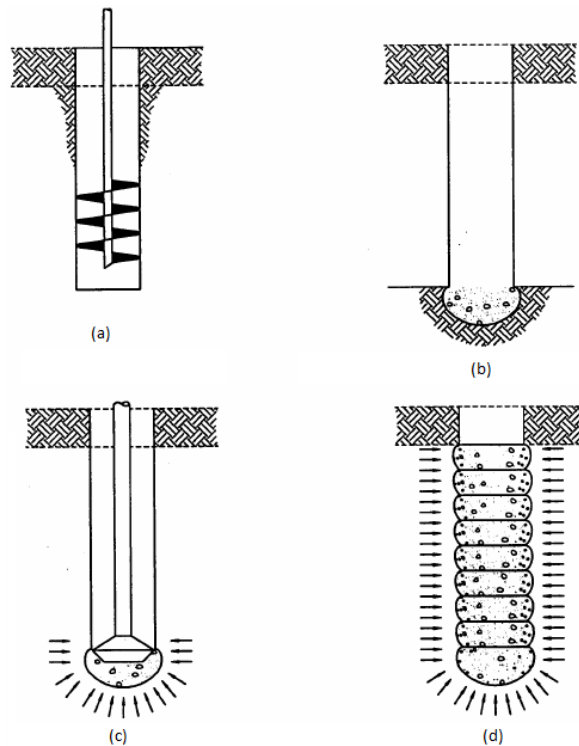


Figure 2.3 Typical construction process of Geopier (a) Creating creating cavity (b) Making the bottom bulb (c) Building shaft with undulating layers (d) Installation complete (Gaul, 2001)

Although the stone column and the Geopier column techniques seem to be similar, there exist essential differences between the two methods. These differences are described by Lawton and Fox (1994) as follows:

- Geopier columns are generally short in length, generally 2 to 8 times of their width.
- Geopier columns are constructed by excavation of the soil or penetration of the drill rig as defined for the rammed aggregate pier construction method, whereas the stone columns are constructed by vertical and horizontal vibration. This causes to less change in parameters of the surrounding soil.
- Geopier columns are constructed using specially designed high frequency hammer which creates vertical vibration instead of horizontal vibration technique.
- Geopier columns are constructed by thin layers of stone which results to stress increase in the surrounding soil and deformations, and also compaction.
- Design approach of Geopier columns is more to improve the underlying soil. In some cases the aim is to increase radial drainage more than reinforcing the soil.

**2.2 Ultimate bearing capacity analysis of footing bearing on soils reinforced with rammed stone columns**

Wissmann (1999) examined design methods in order to calculate bearing capacity of Geopier supported footings. The study examines bearing capacity of Geopier columns of different lengths considering single loaded columns and group columns. Stress increase due to the impact effect and also the intersection between Geopier columns are integrated in the approach. The bearing pressure associated with fully mobilized shear strength is defined as the limit equilibrium bearing capacity of the footing.

Simplified approaches and assumptions are generally used due to the complicated load transfer mechanism between applied load and soil-Geopier structure in the design of Geopier reinforced soils. Ultimate bearing pressures are computed using limit equilibrium theories of classical soil mechanics in conjunction with idealized failure geometries. Generally, design principles take the combined structure as springs into consideration. Low stiffness springs which represent the surrounding soil tend to take smaller forces with the same deflection whereas the stiffer springs tend to take higher loads. Those solutions generally neglect the confining influence provided by the loaded footings and adjacent Geopier elements.

**2.2.1 Bearing capacity of soil reinforced with a single rammed stone column**

Lawton (2001) discussed the behavior of single pier failure in three possible mechanisms. These are described as follows:

- a) Bulging failure
- b) General or local shear failure
- c) Punching failure

Barksdale and Bachus (1983) idealized the failure mechanism of single pier in homogeneous soil as in Figure 2.4.

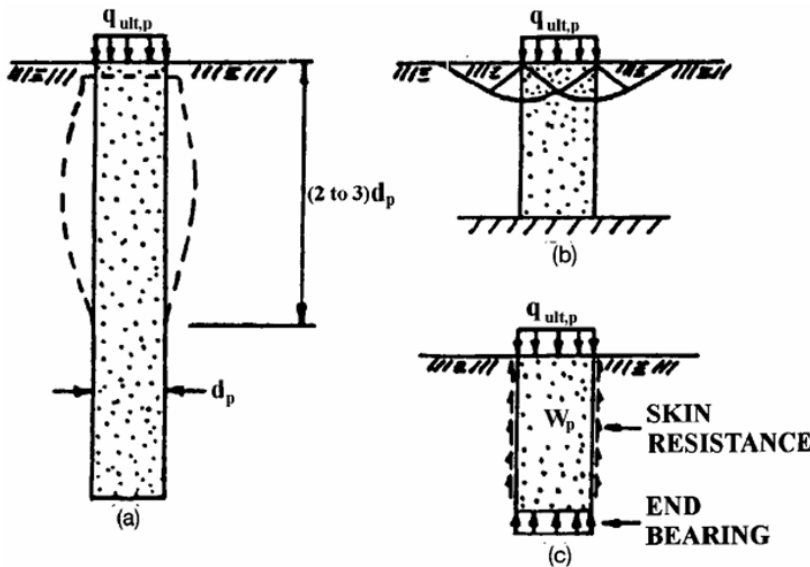


Figure 2.4 Failure mechanisms for single pier in homogeneous soil: (a) Bulging, (b) General or local shear (c) Punching (Barksdale and Bachus, 1983)

Those failure mechanisms are dependent on the confining effect of the surrounding soil as well as the soil beneath the layer where columns are resting. Local or general shear failure may occur through the pier and matrix soil. This may occur in the following two cases: if a very short pier [ $H_p < (2 \text{ to } 3)d_p$ ] bears on a rigid base where  $H_p$  is the length of the pier and  $d_p$  is the diameter of the pier, or if the pier is not much stronger than the surrounding matrix soil. The Local or general shear failure mechanism is similar to shallow foundation failures in unreinforced soils. Punching failure or shearing below the pier is a failure mechanism that occurs when the applied load is greater than the skin friction that develops along the surface of the pier, end bearing resistance, or a combination of both. If the soil is layered, it may only bulge in the weakest layer or in a combination of weaker layers anywhere along the pier where the induced horizontal stresses are greater than lateral resistance of the matrix (Lawton and Warner, 2004).

### 2.2.1.1 Bulging failure of individual rammed stone columns

The potential for the bulging failure of individual granular columnar elements in saturated clays is described by Mitchell (1981). It is stated that if sufficient pressure is applied to the tops of stone columns, the shear strength could be fully mobilized within the elements and along surfaces extending through the surrounding soil matrix. Due to the development of shearing surfaces within the columns, these columns tend to bulge outward. This bulging is resisted by the lateral earth pressure. Bulging occurs when the induced horizontal stress in a pier is greater than the lateral resistance of the matrix soil. Generally, it can be considered that bulging failure may occur at the upper side of the Geopier elements due to the increase of lateral soil pressure with depth.

Hughes and Withers (1974) used the cavity expansion theory in order to formulate an expression for the bearing capacity of single granular elements. This theory assumes that the Geopier aggregate material is non-cohesive. The shear forces associated between column and surrounding soil interface is neglected. Principal stresses are those which act horizontally and vertically (Lawton and Warner, 2001).

Hughes and Withers (1974) idealized bulging of the column like the expanding of a cylindrical gap in clay as like in the pressuremeter test. They used a model in soft normally consolidated clay (kaolinite which has a shear strength of 19.1 kPa) and showed that bulging occurs in depths 2 to 3 times the width of the column below the surface. In this model, 150 mm in length sand columns were used with 12.5 mm to 38 mm diameters. This experimental study showed that forces acting on the column are transmitted to soil due to expanding and vertical movement of the column. It is observed that the column material pressurized the surrounding soil. Both field and laboratory investigations which are shown in Figure 2.5 showed geometrically similar deformation results.

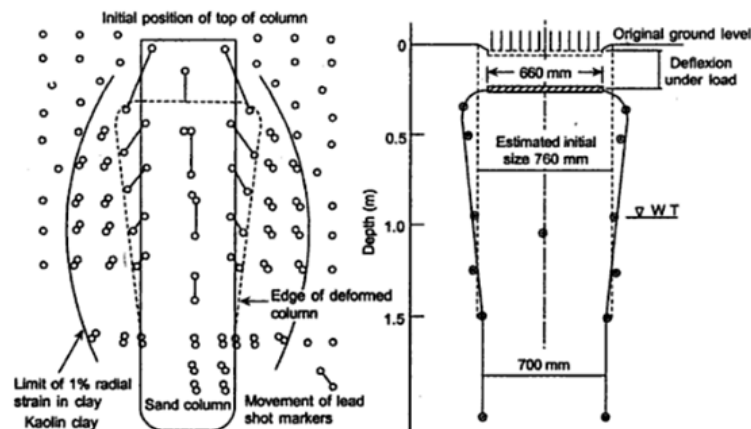


Figure 2.5 Deformation of stone column (Hughes and Withers, 1974)

Hughes and Withers (1974) thought that bulging failure in a single column is similar to the forming of a cavity in a pressuremeter test. The total radial stress after the installation of the rammed stone columns is the sum of the effective radial stress and the pore water pressure. Total radial stress can be calculated from the following equation:

$$\sigma_{r0} = \sigma'_{v0} K_p + u_0 \quad (2.1)$$

where,

$\sigma_{r0}$ : total radial stress

$K_p$ : Rankine passive earth pressure coefficient

$\sigma'_{v0}$ : initial vertical effective stress

$u_0$ : pore water pressure

The elasto-plastic theory developed by Gibson and Anderson (1961) showed that by idealizing the soil as an elasto-plastic material, limit radial stress can be calculated as follows:

$$\sigma_{r,lim} = \sigma_{r0} + c_u \left( \ln \frac{E_s}{2c_u(1 + \nu)} \right) \quad (2.2)$$

where,

$\sigma_{r,lim}$ : limit radial stress

$E_s$ : modulus of elasticity of the soil

$\nu$ : Poisson's ratio

$c_u$ : undrained cohesion of the soil

Using the plasticity theory, the ultimate stress on a singular column is equal to the coefficient of passive earth pressure  $K_{p,g}$  of the stone column, times the lateral limiting radial stress.

The ultimate bearing pressure of a single rammed stone column element can be estimated as the product of Rankine's passive earth pressure and limiting radial stress:

$$q_{ult} = \sigma_{r,lim} K_{p,g} = \sigma_{r,lim} \tan^2 \left( 45 + \frac{\theta_g}{2} \right) \quad (2.3)$$

where,

$\theta_g$ : internal friction angle of the rammed stone column aggregate material

$K_{p,g}$ : passive earth pressure coefficient of the rammed stone column

Vesic, 1972 derived a solution for a cylindrical cavity expansion in an infinite soil mass. As shown in Figure 2.6, around a cylindrical cavity the soil can be divided into a plastic zone and an elastic zone. Figure 2.7 represents cavity expansion factors, depending on the rigidity index.

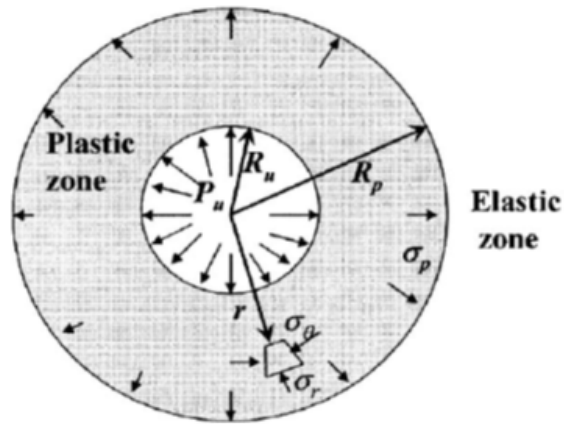


Figure 2.6 Expansion of cylindrical cavity (Vesic, 1972)

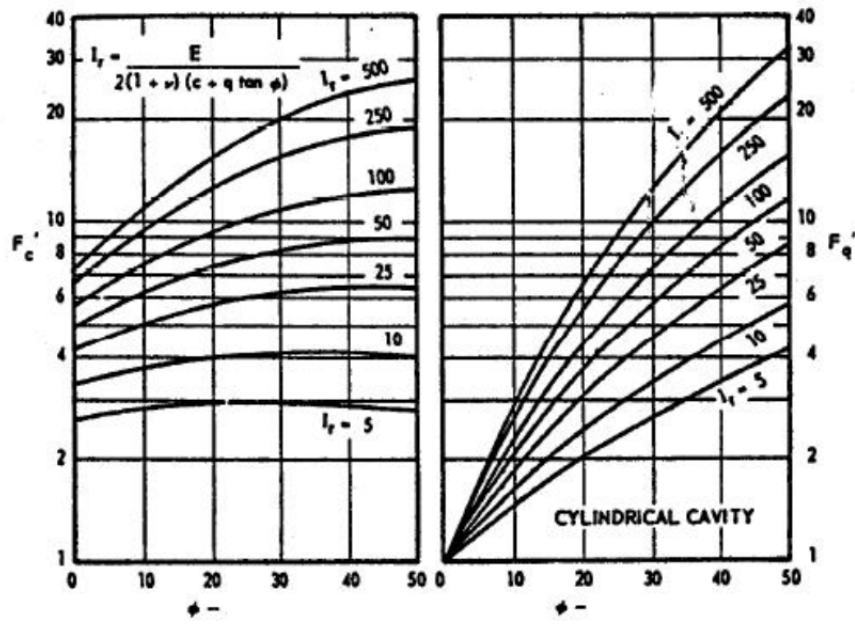


Figure 2.7 Cavity expansion factors (Vesic, 1972)

Vesic, (1972) defined the rigidity index as follows:

$$I_r = \frac{E_s}{2(1 + \nu)(c_u + q \tan \phi_s)} \quad (2.4)$$

$I_r$ : rigidity index

$E_s$ : elastic modulus of the soil

$\phi_s$ : internal friction angle of the soil

$\nu$ : Poisson's ratio of the soil

$q$ : average normal stress at calculated depth where bulging failure is thought to occur

Limiting radial stress due to surrounding soil is calculated as follows:

$$\sigma_3 = c_u F'_c + q F'_q \quad (2.5)$$

and at failure of the column, the following equation can be derived:

$$\frac{\sigma_1}{\sigma_3} = \frac{1 + \phi_g}{1 - \phi_g} \quad (2.6)$$

where,

$c_u$ : undrained cohesion of clay

$F'_c, F'_q$ : cavity expansion factors

$\sigma_1$ : ultimate vertical stress

$\sigma_3$ : limiting radial stress

The bulging depth of the column can be described as:

$$z_b = d_f + \frac{1}{2} d \tan\left(45 + \frac{\phi_g}{2}\right) \quad (2.7)$$

where,

$z_b$ : depth at which bulging occurs

$d_f$ : depth of foundation

$d$ : nominal diameter of the constructed column

Because the Rankine soil stress does not include the vertical limit stress due to the foundation and generated additionally normal and shear stresses during installation of the piers, calculated depth can be considered to be conservative (Wissmann, 1999).

Effective radius of the column shaft is estimated to be approximately 0.076 m greater than the nominal shaft radius as a result of ramming the aggregate stone laterally during densification. Here  $d_{\text{shaft}}$  can be calculated as follows:

$$d_{\text{shaft}} = d + 0.076 \quad (2.8)$$

where,

$d_{\text{shaft}}$ : actual shaft diameter of the column after damping

$d$ : nominal shaft diameter

### 2.2.1.2 Shearing failure below tips of individual rammed stone columns

The total load applied to the top of the columns is resisted by both shaft friction and tip resistance of the columns. Wissmann (1999) neglected own weight of the column and described the equation as follows:

$$Q_{\text{top}} = Q_{\text{shaft}} + Q_{\text{tip}} \quad (2.9)$$

The equation can be re-written in terms of stresses:

$$q_{\text{ult}} = f_s \frac{A_{\text{shaft}}}{A_g} + q_{\text{tip}} \quad (2.10)$$

$$Q_{\text{ult}} A_g = f_s A_{\text{shaft}} + q_{\text{tip}} A_g \quad (2.11)$$

where,

$q_{\text{ult}}$ : ultimate bearing pressure

$q_{\text{tip}}$ : stress resisted at tip of the column

$Q_{\text{top}}$ : total load applied to the top of column

$Q_{\text{shaft}}$ : shaft friction

$Q_{\text{tip}}$ : end bearing of column

$A_g$ : cross sectional area of column

$f_s$ : average unit friction along the shaft

$A_{\text{shaft}}$ : area of the column shaft

Bearing capacity can be calculated for the drained and undrained conditions.

Undrained conditions:

The average unit friction along the shaft of the column ( $f_s$ ) can be considered as the average undrained cohesion of the matrix soil enclosing the column shaft.

$$f_s = c_u \quad (2.12)$$

where,

$f_s$ : average unit friction along the shaft

The expression for the tip bearing capacity in clay soils can be simplified to Meyerhof (1976):

$$q_{tip} = cN_c \quad (2.13)$$

where,

$N_c$ : bearing capacity factor which can be taken nine for clayey soils

Drained conditions:

The average unit friction along the shaft is the product of the average effective horizontal pressure and the tangent of the friction angle of the matrix soil.

$$f_s = \sigma'_{v,avg} K_p \tan(\theta_s) \quad (2.14)$$

$$f_s = (d_f + \frac{H_{shaft}}{2}) \gamma_s K_p \tan \theta_s \quad (2.15)$$

where,

$\sigma'_{v,avg}$ : effective vertical stress at midpoint of the shaft length

$K_p$ : Rankine passive earth pressure coefficient

$d_f$ : depth of the bottom of the footing below adjacent grade

$\gamma_s$ : unit weight of the soil

The tip resistance is calculated from the following equation:

$$q_{tip} = cN_c + \frac{1}{2} d_{shaft} \gamma_s N_y + \sigma'_{v,tip} N_q \quad (2.16)$$

where,

$c$ : cohesion of the soil

$\gamma_s$ : unit weight of the soil

$N_q$  and  $N_y$  bearing capacity factors

$\sigma'_{v,tip}$  is the overburden stress at the elevation of the tip of the column

Lawton et al. (1994) discussed that shear stresses which develop during loading of the pier are ignored in this equation. Mohr's circle indicates that if a vertical force is applied to the pier, shearing stresses develop along the pier matrix-soil interface, which causes a rotation of the principal stresses and an arch in the soil (Handy, 1985).

The calculations tend to be conservative due to the following reasons:

- They do not include vertical confining stresses provided by the overlying loaded footing

- They account only for three inches of radial expansion during column installation

### 2.2.2 Bearing capacity of soil reinforced with a rammed stone column group

The failure of a group of columns in essence is similar to that of a single column. A number of failure mechanisms are identified such as bulging, local shear within the reinforced matrix, punching below the single column or shear below the reinforced matrix zone. Hughes and Withers (1974) indicated that stone columns act independently if the spacing between two columns is greater than about  $2.50d$ . Fox and Cowell (1998) described the failure mechanisms in pier groups as in Figure 2.8.

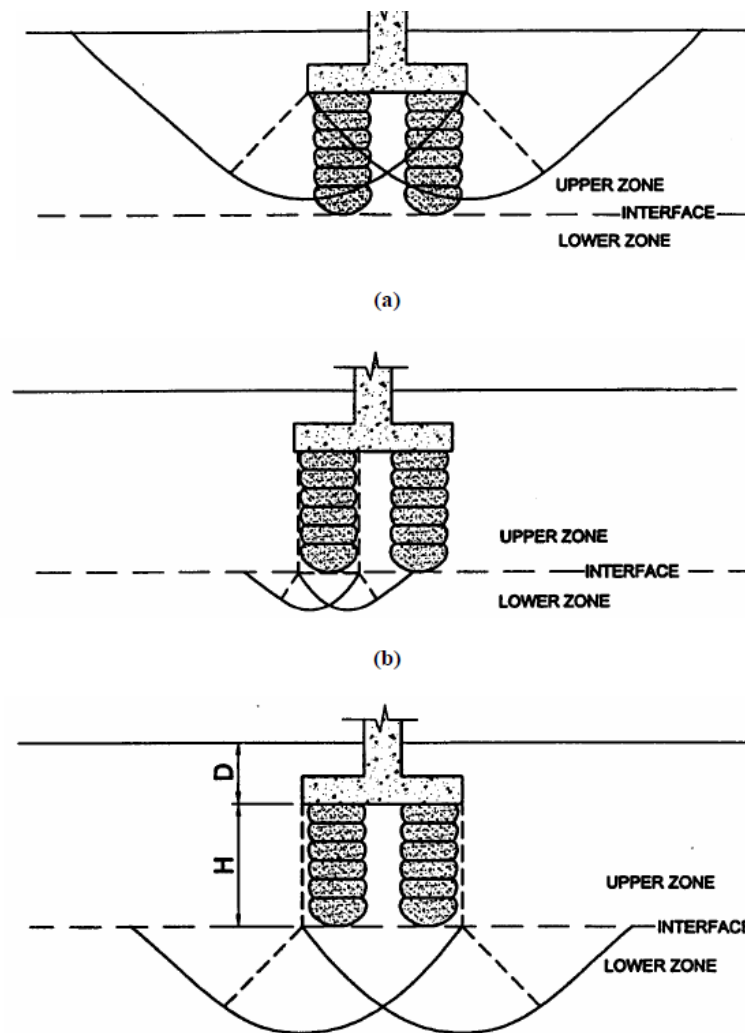


Figure 2.8 Possible failure mechanisms in Geopier groups: (a) Local shear within pier-reinforced matrix zone; (b) Individual punching; and (c) Shearing below pier-reinforced matrix zone (Fox and Cowell, 1998)

### 2.2.2.1 Shearing failure within reinforced soil zone

This approach assumes that shearing occurs within the reinforced part through the shear planes crossing the columns within the soil matrix. Mitchell (1981) summarizes approaches formulated by Priebe (1978) and Aboshi et al. (1979) that use composite shear strength parameters to provide solutions for this condition. Composite shear strength parameter of the compacted stone column elements and the surrounding soil can be used to calculate bearing capacity of the total system via classical Terzaghi-Buisman bearing capacity equation.

Priebe's (1978) recommendation for the calculation of the composite friction angle of the reinforced soil ( $\phi_{\text{comp}}$ ) and composite cohesion intercept ( $c_{\text{comp}}$ ) are as follows:

$$\phi_{\text{comp}} = \tan^{-1}[R_a n \tan \phi_g + (1 - R_a n) \tan \phi_s] \quad (2.17)$$

$$c_{\text{comp}} = (1 - R_a n)c \quad (2.18)$$

$R_a$ : ratio of the area coverage of the columns to the gross area of the soil matrix in the area subject to shearing

$n$ : ratio of the stress applied to the columns to the stress applied to the matrix soil

Priebe (1978) and Aboshi et al. (1979) approaches can be implemented by using the expressions shown in Equations 2.17 and 2.18 above, provided that the effects of Geopier and failure plane geometry and the effects of Geopier stress reductions with depth are considered. To account for shearing planes that extend beyond the footprint of the concrete foundation, it is recommended that  $R_a$  be estimated by modifying the compacted stone column/footing coverage area ratio (typically about 0.33) by a reduction factor of 0.4.

$$R'_a = 0.40R_a \quad (2.19)$$

where,

$R_a$ : area replacement ratio

$R'_a$ : area replacement ratio which is calculated by multiplying by reduction factor of 0.40

$\phi_{\text{comp}}$ : composite internal friction angle

$c_{\text{comp}}$ : composite cohesion

Soil can be densified by the applied stress; however this effect is not well understood. It is conservative to ignore this effect so that the composite unit weight is a function of  $R_a$ ,  $\gamma_p$ , and  $\gamma_m$  only. (Lawton, 2004)

### 2.2.2.2 Unit cell concept for settlement and bearing capacity of a rammed stone column group

In order to calculate settlement and bearing capacity of a rammed stone column and surrounding soil, the improved soil layer has to be considered as a whole. Barksdale and Bachus (1983-a) recommended for the ultimate group capacity for stiffer soils, where "bulging" is not expected to a great degree, to use average strength parameters in combination with the Vesic cylindrical cavity expansion theory.

The idealization of unit-cell concept which is shown in Figure 2.9 (Barksdale and Bachus, 1983) is based on the following assumptions:

- The unit cell is repeated infinitely in the lateral directions
- The load due to the applied uniform pressure at the top of a unit cell remains within that unit cell
- Lateral deformations at the boundaries of the unit cell do not cross the outer edge of the cell due to symmetry of loading and geometry (i.e., one dimensional loading)
- Shear stresses along the outer boundaries of the unit cell are zero.

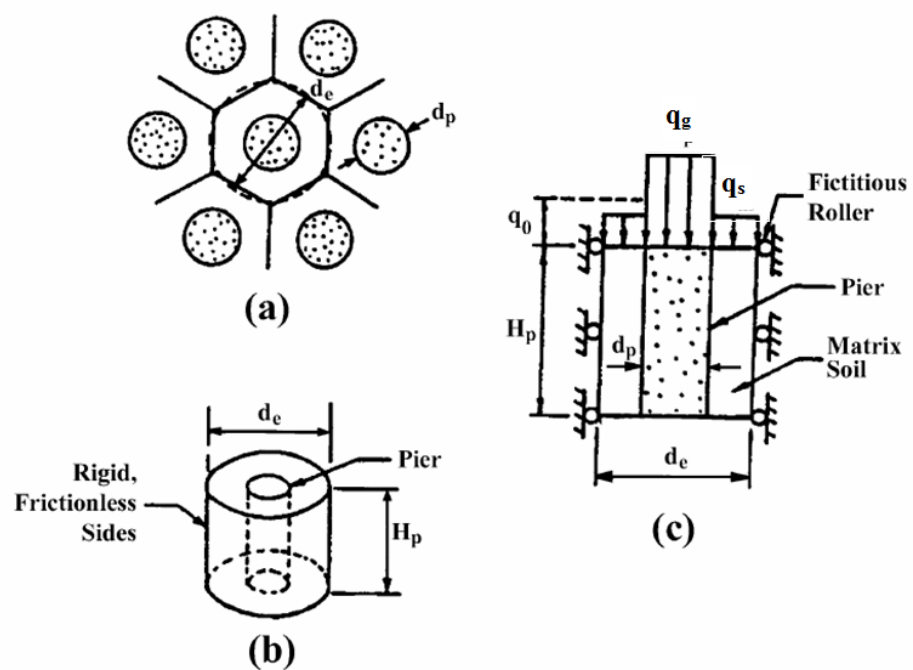


Figure 2.9 Idealization of unit cell: (a) Plan view (b) Unit cell (c) Vertical cross section (modified from Barksdale and Bachus, 1983)

Each column may be considered as a unit cell. For a triangular placement of columns, the equivalent effective diameter can be calculated as follows:

$$D_e = 1.05s_g \quad (2.20)$$

For a square placement of columns, the equivalent effective diameter can be calculated as follows:

$$D_e = 1.13s_g \quad (2.21)$$

where,

$D_c$ : effective diameter of the column

$s_g$ : spacing of individual columns

### 2.2.2.3 Shearing failure below reinforced soil zone

Shearing or general bearing capacity failure may occur below the pier-reinforced matrix zone. The stress induced at the bottom of the reinforced layer ( $q_{\text{bottom}}$ ) is estimated by assuming that load spreading increases at a rate of 2:1 (vertical to horizontal) below the bottom of the footing:

$$q_{\text{bottom}} = q_{\text{ult}} \frac{BL}{(B + H_{uz})(L + H_{lz})} \quad (2.22)$$

where,

B: footing width

L: footing length

$H_{uz}$ : thickness of the reinforced soil layer

$q_{\text{bottom}}$ : ultimate bearing pressure at bottom of reinforced soil

$q_{\text{ult}}$ : footing ultimate bearing pressure

## 2.3 Settlement calculations of footings on soil reinforced with rammed stone columns

Although bearing capacity of the ground seems to be of top priority, sometimes settlement problems may cause unrecoverable hazards to the overlying structures. Depending on the soil type, these settlement durations may take several months or years before the majority of the settlement is completed. Controlling settlement at the design step is critical to prevent such hazards on the structures.

The soil reinforcement settlement control design methodology is based on a two-layer settlement approach as described by Lawton et al. (1994), Lawton and Fox (1994), Fox and Cowell (1998), and Wissmann et al. (2002). This methodology takes the soil into consideration as two different layers. One of these layers is the layer with reinforced zone (upper zone). Figure 2.10 shows the upper and lower zone methodology described by Fox and Cowell (1998). The area below the reinforced zone, referred to as the lower-zone, is evaluated using conventional geotechnical analysis approaches. The total settlement,  $s_{\text{tot}}$  is obtained by summing up evaluated settlement results of the upper zone and the lower zone settlement.

$$s_{\text{tot}} = s_{uz} + s_{lz} \quad (2.23)$$

where,

$s_{uz}$ : upper zone settlement

$s_{lz}$ : lower zone settlement

The total settlement of the reinforced footing is described by Fox and Cowell (1998) by the following equation:

$$s_t = s_{i,uz} + s_{i,lz} + s_{c,lz} + s_{m,lz} \quad (2.24)$$

where,

$s_{i,uz}$ : immediate settlement of the upper zone

$s_{i,lz}$ : immediate settlement of the lower zone

$s_{c,lz}$ : settlement from primary consolidation of the lower zone

$s_{s,lz}$ : settlement from secondary consolidation of the lower zone

$s_{m,lz}$ : settlement from changes in moisture within the lower zone

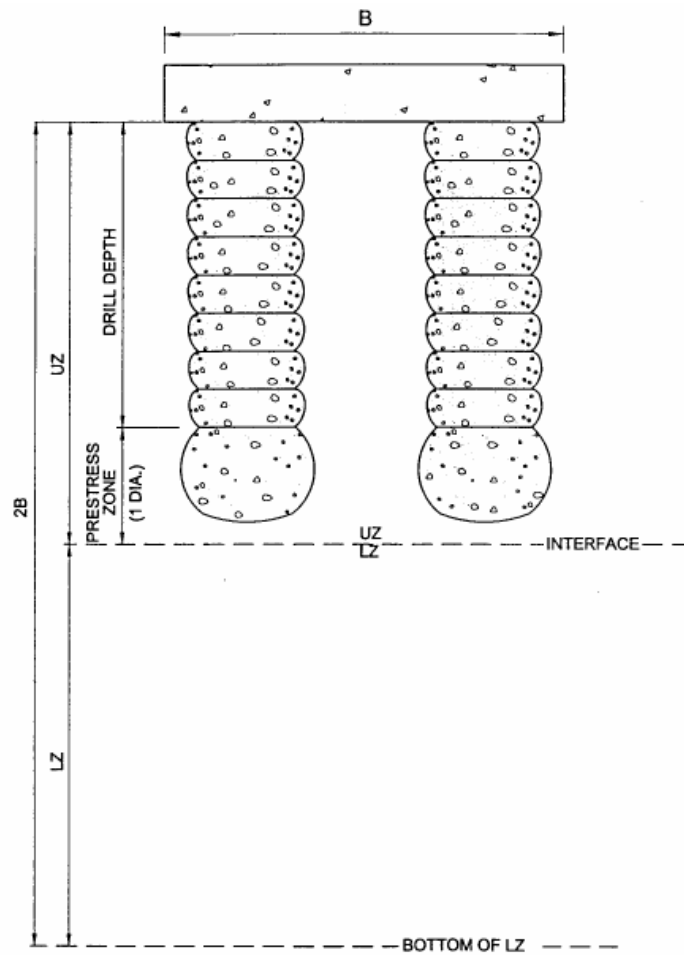


Figure 2.10 Upper zone and lower zone beneath an isolated footing (from Fox and Cowell, 1998)

The upper zone of the soil is described as the summation of the shaft length of the column and shaft diameter of the column.

$$H_{uz} = H_{shaft} = H_0 + d_{shaft} \quad (2.25)$$

The lower zone of the soil is calculated as follows:

$$H_{LZ} = 2B - H_{shaft} = 2B - H_0 - d_{shaft} \quad (2.26)$$

where,

$H_{Lz}$ : lower zone layer thickness

$H_{uz}$ : upper zone layer thickness

$H_0$ : nominal length of column

$d_{shaft}$ : actual shaft diameter of the column after damping

$B$ : footing width

### 2.3.1 Evaluation of the stress concentration ratio

Due to the difficulty in determining the mean stress acting on the aggregate pier as a result of its higher stiffness relative to the native soil, Aboshi et al. (1979) recommended an analytical equation by the stress concentration ratio. He put forward that when loading is applied onto the composite ground, stress re-distribution occurs between the stone column element and surrounding soil. This stress concentration ratio can be calculated as follows:

$$n = \frac{\sigma_g}{\sigma_s} \quad (2.27)$$

where,

$n$ : stress concentration ratio

$\sigma_g$ : effecting vertical stress on the column

$\sigma_s$ : effecting vertical stress on the cohesive soil

Average stress occurring at a specific depth in the unit cell can be calculated as follows:

$$\sigma_{avg} = \sigma_g R_a + \sigma_s (1 - R_a) \quad (2.28)$$

where,

$R_a$ : area replacement ratio

Wiessmann (1999) recommends 2.8 for the ratio of the stress applied to the Geopier elements to the stress applied to the matrix soil. The implementation of these conditions results in a soil matrix stress concentration factor of 2.8, which accounts for both depth and shear plane orientation considerations. Barksdale and Bachus (1983) presented results of stress concentration ratios obtained from several field tests in Table 2.1.

Table 2.1 Observed stress concentration ratios on stone columns (Barksdale and Bachus, 1983)

Type of test	Alignment	Stress concentration ratio (n)	Change in time	Length of stone column (m)	Type of soil
Fill	Square s = 1.7m D = 0.9m a <sub>s</sub> = 0.25	2.8 (average)	Nearly constant	6.7 – 7.9	Soft clay
Load test	Equilateral triangle s = 1.8m D = 1.2m a <sub>s</sub> = 0.43	3.0 (start) 2.6 (end)	Decreasing	6.3	Very soft and soft sandy silty clay
Try fill	Square s = 2m D = 1.1m a <sub>s</sub> = 0.26	2.6 – 2.4 (start) 4.0 – 4.5 (end)	Increasing	20	Soft clay, silt and sand with organic content
Fill	Square s = 0.1– 0.3	4.9 (average)	Increasing	variable	Very soft and soft sediment
Model test	Square D = 0.03m a <sub>s</sub> = 0.07 – 0.4	1.5 – 5	Constant	variable	Soft clay

### 2.3.2 Immediate settlement of the upper zone

The settlement of the upper zone is based on the composite stiffness of the compacted stone columns and densified matrix soil surrounding pier. The upper zone analysis method uses a spring analogy which is shown in Figure 2.11 and considers the stiff column acting as a stiff spring, while the less stiff matrix soil acts as a soft spring (Lawton et al., 1994). The height of the upper zone is the length of the column plus one diameter.

In the stiff spring analogy, the stiffer springs represent the stiffer rammed stone columns material where softer springs represent the matrix soil. Under an applied load on a rigid footing which rests on the springs, all springs will deflect the same amount. From fundamental physics, the magnitude of the resisting force generated within a spring (P) is directly proportional to the magnitude of  $\delta$ , as in the following equation:

$$P = -k\delta \quad (2.29)$$

where,

P: applied load

k: stiffness

$\delta$ : displacement

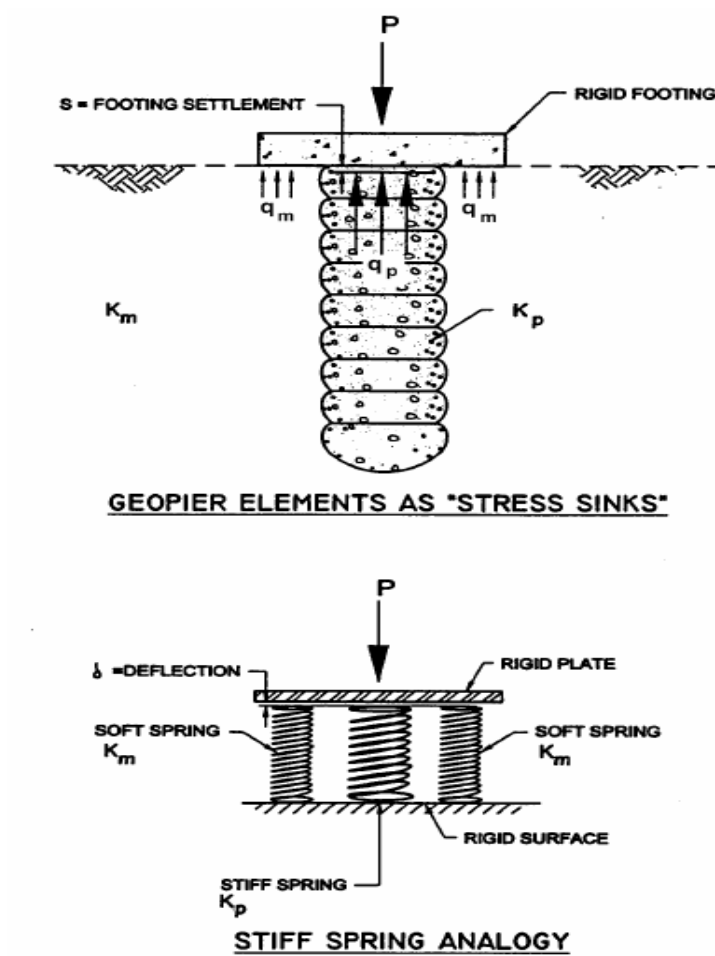


Figure 2.11 Spring analogy for stress concentration along interface of footing and Geopier-reinforced bearing soil (modified from Fox and Cowell, 1998)

Due to the low k value of the matrix soil, the resisting force generated by the soil will be lower than the force generated by the stiffer springs. Summing forces in the vertical direction for the upper part gives the following equation:

$$\Sigma F_v = 0 = q_0 A - q_g A_g - q_s A_s \quad (2.30)$$

The total vertical stress due to the applied pressure at a given depth must equilibrate for strain compatibility, as such follows:

$$q_g = \frac{q_0 n}{R_a(n-1) + 1} \quad (2.31)$$

$$q_s = \frac{q_0}{R_a(n-1) + 1} \quad (2.32)$$

where,

$F_v$ : vertical force

$q_0$ : average applied stress

$q_g$ : top of column stress

$q_s$ : top of soil stress

$n$ : stress concentration ratio

$R_a$ : area replacement ratio

It is recommended to use the nominal area of the compacted stone column and not to include the increase in size of the pier due to the compaction process.

The equation derived to express the upper zone settlement component is by accepting the foundation as fully rigid as follows:

$$s_{uz} = \frac{q_g}{k_g} = \frac{q_s}{k_s} \quad (2.33)$$

where,

$k_g$ : stiffness of rammed stone columns

$k_s$ : stiffness of the soil matrix

Settlement of the surrounding soil will be equal to the settlement of the rammed stone columns. The upper zone settlement methodology provides for a determination of the deflection of the rammed stone column, but not of the matrix soil between the piers.

Field instrumentation results, however, show that only minor differential settlement is observed between the top of the rammed aggregate pier and the matrix soil under embankment loadings (Minks, 2001; White, 2002).

### 2.3.3 Immediate and consolidation settlement of the lower zone

The basic assumption inherent in the approach is that the footing is perfectly rigid compared with the matrix soil and the column element. Estimates of settlement components from the lower zone soils are computed using conventional geotechnical settlement analysis methods that rely on estimating the degree of load spreading below the footing and estimating the compressibility of the soils. The analysis includes the assumption that vertical stress intensity within the lower zone is the same as that of a bare footing without the stiffened upper zone, using solutions for a footing supported by an elastic half-space. This assumption is considered to be conservative because the presence of the stiff pier results in a stress concentration on the pier, and a more efficient stress transfer with depth below the footing bottoms than what would occur for conventional bare footings. This has been shown during full scale pier-supported footing tests that were instrumented with pressure cells (Lawton, 1999). Consisting of either elastic settlement analyses or consolidation analyses using the equations below:

$$s_{lz} = \frac{\Delta_q H_{lz} I_q}{E} \quad (2.34)$$

$$s_{lz} = \left[ \frac{1}{1 + e_0} \right] H \times \log \left[ \frac{p_0 + \Delta q}{p_0} \right] \quad (2.35)$$

$$s_{i,lz} = A_1 \times A_2 \frac{q_0 B}{E} \quad (2.36)$$

where,

for square or circular foundations;

$s_{i,lz}$ : immediate settlement of the lower zone

$e_0$ : initial void ratio

$q_0$ : average applied stress

$\Delta_q$ : stress increment

$I_q$ : Westergaard effect factor

$E$ : Elastic modulus of the soil

$A_1$  and  $A_2$ : elastic settlement factors to be taken from Figure 2.12

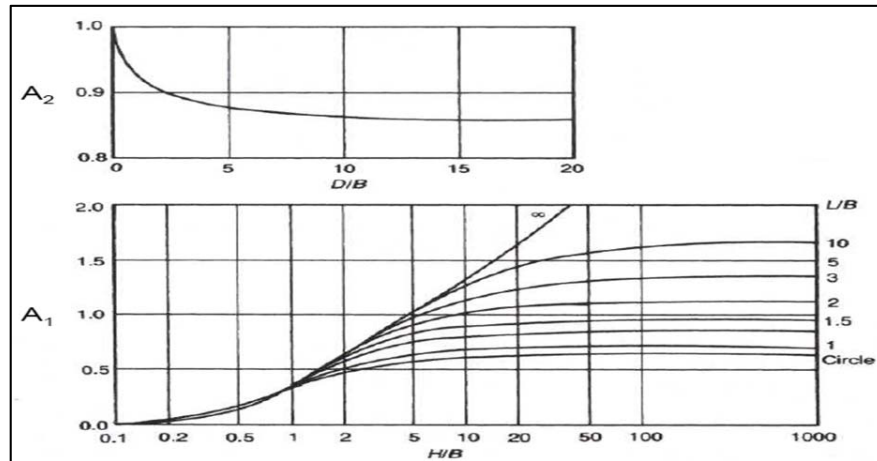


Figure 2.12 Factors to be used for the calculation of elastic settlement (Christian and Carrier, 1978)

## 2.4 Strength parameters of rammed stone column material

Several methods in the past studies have been suggested for the estimation of strength parameters of constructed columns. Further, multiple tests have been carried out on Geopier columns in order to reveal those parameters for different gradations of material.

### 2.4.1 Shear strength of construction material

Small scale laboratory triaxial tests performed on reconstituted samples demonstrate that the angle of internal friction for Geopier aggregate ranges from  $49^\circ$  to  $52^\circ$ , depending on variations in gradation. Results obtained from direct shear tests performed on Geopier elements (Fox and Cowell, 1998) are shown in Figure 2.13.

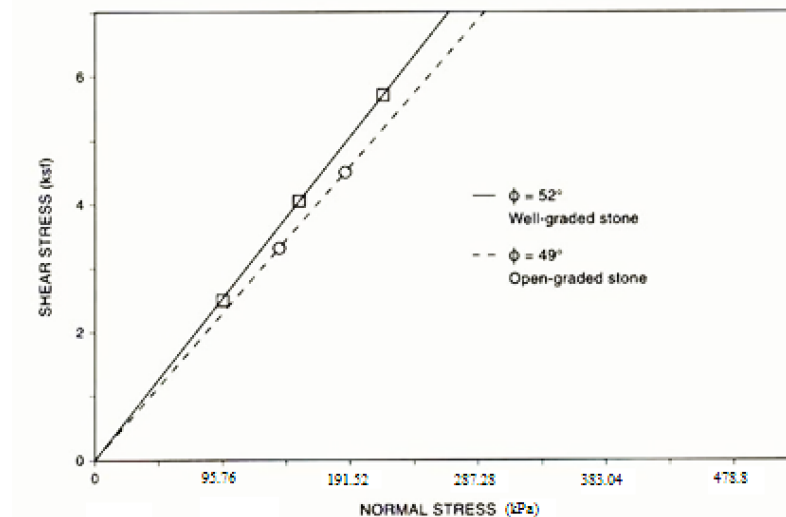


Figure 2.13 Results obtained from full-scale direct shear tests performed on Geopier elements (modified from Fox and Cowell, 1998)

Small-scale laboratory triaxial tests were performed at Iowa State University on reconstituted samples of well-graded Geopier aggregate compacted to densities consistent with those measured for installed Geopier elements (White, 2001). Test results, which are shown in Figure 2.14 indicate an angle of internal friction of  $51^\circ$ .

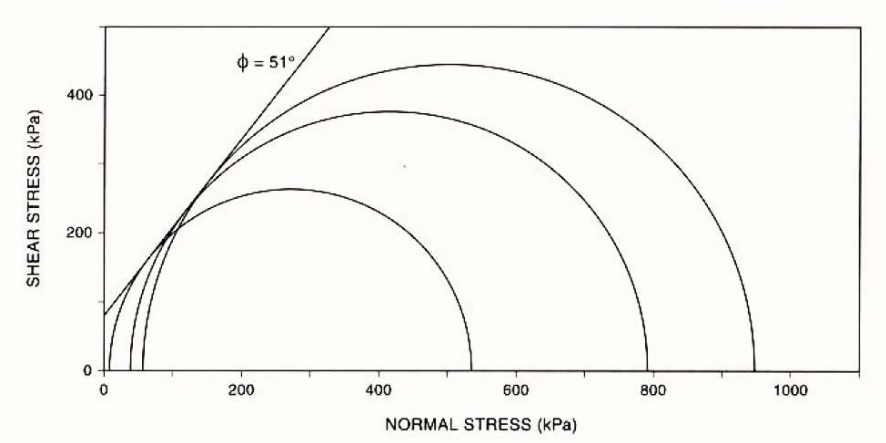


Figure 2.14 Small-scale laboratory triaxial tests results on reconstituted samples of well-graded Geopier aggregate compacted to densities consistent with those measured for installed Geopier elements (White, 2001)

Wissmann et al. (1999) analyzed the shear strength of Geopier columns in relation with the bearing capacity and settlement control. In order to reveal the properties of Geopier columns, they conducted direct shear tests on field and some triaxial tests in laboratory. Direct shear test results show that following the Geopier column constructions, the internal friction angle is  $49^\circ$ , where fines content is zero; and the internal friction angle is  $52^\circ$ , where fines content is 10%. Triaxial test results showed that the internal friction angle, where fines content is 10%,  $51^\circ$ , is similar to the results obtained on field.

**2.4.2 Modulus of subgrade reaction for single rammed stone column**

Fox and Cowell (1998) provided Table 2.2 from several modulus tests that can be used to estimate the stiffness modulus of Geopier based on the standard penetration test (SPT) blow counts, which can be used for an initial design.

Table 2.2 Typical Geopier design parameter for peat and organic foundation soils (Fox and Cowell, 1998)

Soil classification	SPT N-value	UCS (kN/m <sup>2</sup> )	Geopier element support capacity (cell capacity) $q_{cell}$ (kN)	( $k_g$ ) Geopier stiffness modulus (MN/m <sup>2</sup> )
Peat	1-3	10-48	133	20
	4-6	48-110	200	30
	7-9	110-168	245	34

Alternatively, the modulus of subgrade reaction of a rammed stone column element can be calculated from the results of a static plate load test (ASTM D 1143-81). Figure 2.15 presents the plate load test setup described by Bowles (1996). Load settlement curves of several tests indicated that if the applied load becomes larger the relationship between load and settlement becomes non-linear.

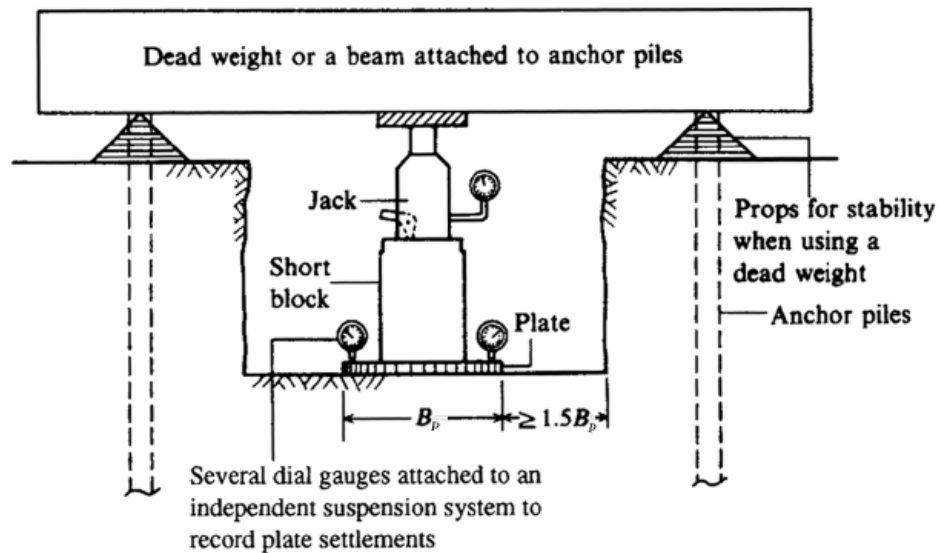


Figure 2.15 Plate load test setup (Bowles, 1996)

Terzaghi (1955) gave scaling relationships for two cases. He stated that if the deformation characteristics were more or less independent of depth, like those of stiff clay, it could be assumed that the settlement increases in simple proportion to the depth of the bulb of pressure. Therefore, the subgrade modulus of full-scale footings on stiff clays or other soils whose stiffness is more or less independent of depth, can be related to the subgrade modulus from the plate load test expressed as follows:

$$k_m = k_{mp} \frac{B_p}{B_{fs}} \quad (2.37)$$

where,

$k_{mp}$ : modulus of subgrade reaction determined from square plate load test

$k_m$ : modulus of subgrade reaction of full-scale footing

$B_p$ : width of square loading plate

$B_{fs}$ : width of full-size footing

Suleiman and White (2006) proposed the following relationship for the evaluation of the elasticity modulus of rammed aggregate piers ignoring the stresses created between the pier and the soil.

$$E = \frac{P_{avg,g} L_t}{A_g \Delta L_t} \quad (2.38)$$

where,

$P_{avg,g}$ : average measured load in the pier obtained using the measured load at the top and bottom of the pier

$L_t$ : distance of telltale plate to top plate

$A_g$ : cross-sectional area of the column

$\Delta L_t$ : measured shortening length of the column at each loading step

## 2.5 Determination of ultimate bearing capacity from stress-settlement data

To be able to confirm the validity of calculations pertaining to the rammed stone columns, field tests can be carried out. Recommendations are available in literature to be followed during testing and evaluation of the test results. Vesic (1975) recommended that using load-settlement curves from a load test, the ultimate load can be defined where the slope of the load-settlement curve becomes zero, or reaches a minimum as in the case of curves 2 or 3 in Figure 2.16 which shows the typical shapes of the constructed load test on field. Vesic (1973) provided guidelines which gave approximate failure limits for different types of soil. These are 3% to 7% of the footing width in saturated clay.

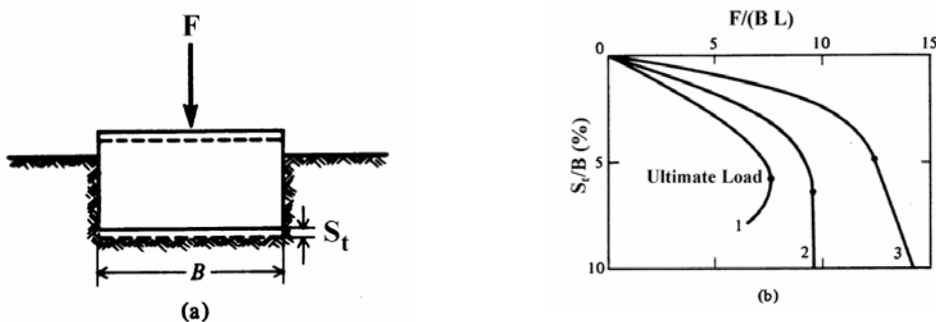


Figure 2.16 Determination of ultimate bearing stress from settlement data: (a) Footing showing nomenclature, (b) Sample load-settlement curves (modified from Vesic, 1975)

Several other methods exist, using which the ultimate bearing capacity can be calculated using settlement-load curves. These methods are briefly described below.

### 2.5.1 Chin-Kondner method

The method proposed by Chin (1970,1971) assumes that the relationship between load and settlement is hyperbolic. The measured settlement values are divided by corresponding loads. This method determines the load-displacement curve for which the Chin-Kondner plot is a straight line throughout. Figure 2.17 shows the load-settlement curve of an axially loaded continuous flight auger pile.

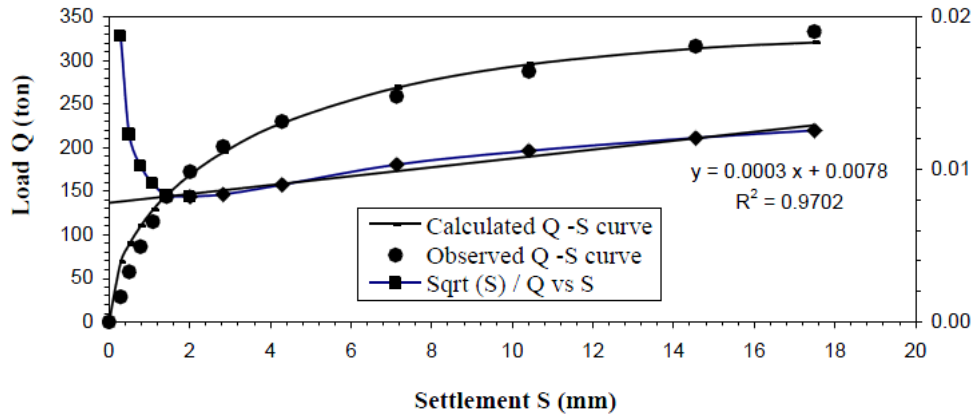


Figure 2.17 Load-settlement curve of an axial loaded continuous flight auger pile (Abdelrahman, et al., 2003)

The following equation can be derived from the plot:

$$\frac{s}{Q_u} = c_1 s + c_2 \quad (2.39)$$

$$Q_u = \frac{1}{c_1} \quad (2.40)$$

where,

s: settlement

$c_1$ : slope of the straight line

$c_2$ : y-axis intercept of the straight line

$Q_u$ : estimated ultimate load

### 2.5.2 Mazurkiewicz's method

Mazurkiewicz (1972) suggested a method of extrapolating the curve of load settlement. This method assumes that the load-settlement curve is approximately parabolic. Measurements are taken and plotted against load. The settlement lines are arbitrary chosen using equal intervals and corresponding loads are marked on the abscissa. 45-degree lines are drawn from the load axis to intersect with the next vertical line running through the next load point. A straight line is drawn through this intersections which jointing with the load axis defines the ultimate load. Figure 2.18 represents the load-settlement curve of a axial loaded continuous flight auger pile, where pile ultimate load is calculated using Mazurkiewicz’s method.

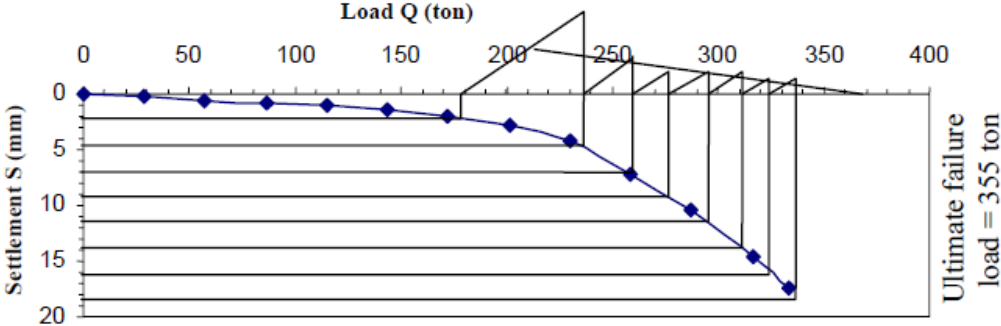


Figure 2.18 Estimation of ultimate failure load according to Mazurkiewicz (Abdelrahman et al., 2003)

**2.5.3 Decourt’s extrapolation method**

Decourt (1999) proposed a method, where each load is divided by its corresponding settlement and the results are plotted against the applied load. By assuming the curve as to be linear, the slope and y-axis intersections can be obtained. Decourt accepted the ultimate load as to be the ratio between the y-intercept and the slope of the line. Linear regression over the apparent straight-line determines the required slope  $c_1$  and y- intercept  $c_2$  constants. Figure 2.19 represents the the estimation of the ultimate bearing capacity of a pile load test for continuous flight auger pile. Ultimate bearing capacity of the pile can be calculated as the ratio between the y-intercept and the slope of the line which is given in below:

$$Q_U = \frac{c_2}{c_1} \tag{2.41}$$

where:

$c_1$ : slope of the straight line

$c_2$ : y-axis intercept of the straight line

$Q_u$ : estimated ultimate load

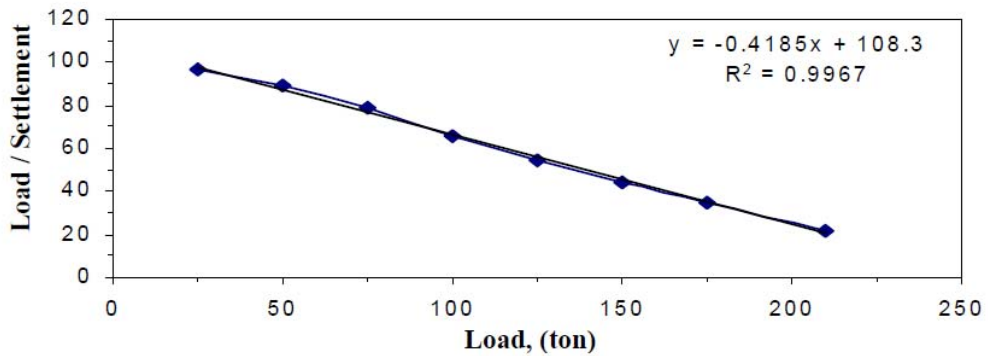


Figure 2.19 Estimation of ultimate failure load according to Decourt's extrapolation method (Abdelrahman et al., 2003)

## 2.6 Classical methods for the bearing capacity calculation

Conventional bearing capacity equations are used in order to evaluate the bearing capacity by using composite strength parameters or calculating the tip resistance of the reinforced soil. One of the widely used bearing capacity equations which was proposed by Terzaghi (1943) is given below:

$$q_{ult} = cN_c s_c + \bar{q}N_q + \frac{1}{2} \gamma B N_\gamma s_\gamma \quad (2.42)$$

where,

$q_{ult}$ : ultimate bearing pressure

$c$ : cohesion of soil

$\gamma_s$ : unit weight of soil

$\bar{q}$ : effective overburden stress at the bearing elevation outside the footprint of the footing

$N_c$ ,  $N_q$  and  $N_\gamma$ : bearing capacity factors

$s_c$  and  $s_\gamma$ : shape factors



## CHAPTER 3

### EXPERIMENTAL AND NUMERICAL STUDY

This chapter presents a case study of foundation soil improvement for a building structure using rammed stone columns system in Çakırlar Çiftliği, Yenimahalle, Ankara, Turkey. The map which indicates the area is given I Appendix A. In the project area, due to the weak local soil conditions and associated settlement problems reported in adjacent structures that were constructed earlier, improvement of foundation soils through appropriate methods is considered for prospective constructions. In the current project, the selected ground improvement method is rammed stone columns system.

Within the framework of the case study, a set of laboratory and field tests are carried out on undisturbed and disturbed soil samples collected from the construction site to define the soil parameters. Test results are reported in this section of the research. Settlement and ultimate bearing capacity calculations of the reinforced soil are evaluated using empirical correlations available in the literature based on the engineering properties of rammed stone column and the subsoil. Design considerations for the rammed stone columns are adopted from improved methods for Geopier systems.

A plate load test is carried out on a single constructed rammed stone column in order to evaluate the relevant elastic parameters of the single column. Another plate load test on a group of closely spaced rammed stone columns is conducted. The schematic cross sectional view of the conducted plate load test on a group of rammed stone columns is presented in Figure 3.1 and Appendix A.

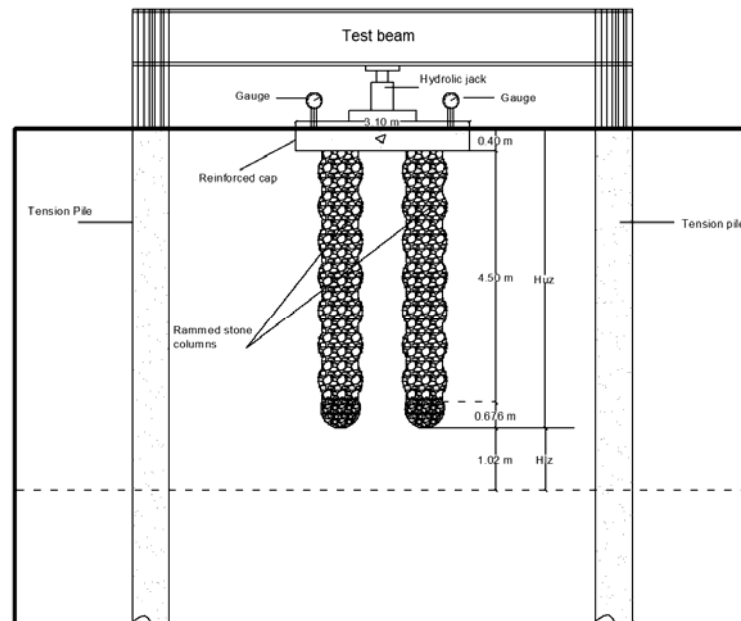


Figure 3.1 Conducted plate load test setup on reinforced soil

Plate load tests in this study are performed in accordance with ASTM D 1143-81 Standard. The design load is calculated using empirical correlations available in the literature.

Finite element model simulation of the group loaded test model is carried out using the program PLAXIS 3D. Settlements are evaluated in the finite element analysis for each load increment and the results are compared to the readings recorded during the test and those calculated based on the empirical correlations.

### 3.1 Classification and engineering properties of the site soils

The geological map of the site is give in Appendix A. The index and engineering parameters of the site soils are identified based on a number of laboratory tests. A set of undisturbed soil samples were procured from the site using Shelby tube samplers. Furthermore, during standard penetration test, representative disturbed soil samples were collected by means of a split spoon. All of the samples were labeled and sealed before being transported to the laboratory for testing.

The tests performed and the relevant standards utilized are listed below:

- Water content (TS 1900-1)
- Atterberg limits (TS 1900-1)
- Sieve analysis (ASTM 2487/90)
- Unit weight (TS 1900-1)
- Triaxial compression test - UU (TS 1900-2)
- Soil classification (ASTM D 2487-11)
- Direct shear test (ASTM D3080/D3080M)

Three 15 m deep boreholes were drilled; observed sub-surface conditions and soil profiles were logged. Standard penetration tests (SPT) and pressuremeter tests were carried out during drilling operations. No groundwater was observed within the investigated depth range. Field observations and classification tests show that the soil profile is mainly composed of clay with some silt and trace of sand. Corrected SPT-N values range between 5 and 17 blows in the uppermost 10 m of the profile and increase to 24-50+ blows below this depth. Boring logs are given in the Appendix A.

According to the sieve analyses, more than 50% of the soil particles passed No.200 sieve. In addition Atterberg limit tests show that the range of the plasticity index is between 14% and 42% with an average of 28%, whereas the range of the liquid limit is between 39% and 76% with an average of 45%. Accordingly, the site soils are classified as the clays of low plasticity (CL) and clays of high plasticity (CH). Natural water content varied within a range between 7% and 31%. Detailed laboratory test results are given in Appendix A. Summary of the subsoil properties is provided in Table 3.1.

In two of the boreholes, pressuremeter tests were performed systematically in every two m intervals from the ground surface to 10 m depth. The net limit pressure values of the clay layers at the site are found to vary between 2.6 kg/cm<sup>2</sup> and 4.0 kg/cm<sup>2</sup>. These values in fact point out that the clay is weak. Moreover, the Menard modulus of elasticity was calculated in the range of 22 kg/cm<sup>2</sup> to 40 kg/cm<sup>2</sup>. Pressuremeter readings are reported in the Appendix A.

Unconsolidated-undrained (UU) triaxial tests and direct shear tests were carried out in the laboratory over undisturbed soil samples which are retrieved from the top 12 m of the soil profile. Average value of the undrained cohesion ( $c_u$ ) is calculated as 48 kPa from (UU) tests. The results of direct shear tests

yielded average values of  $c'$  and  $\phi'$  as 8 kPa and  $25^\circ$ , respectively. Table 3.1 presents the evaluated site soil properties.

Table 3.1 Properties of the site soils

Soil Properties	
dry unit weight, $\gamma'_s$ (kN/m <sup>3</sup> )	17.50
oedometer modulus of elasticity, $E_{oed}$ (kPa)	6461
modulus of elasticity, $E$ (kPa)	4800
Poisson's ratio, $\nu$	0.30
effective cohesion, $c'$ (kPa)	8
undrained cohesion, $c_u$ (kPa)	48
effective internal friction angle, $\phi'$ ( $^\circ$ )	25

### 3.2 Construction of the rammed stone columns

Rammed stone columns were primarily constructed at the site to carry out the load tests. The machine used for the rammed stone column construction is shown at work in Figure 3.2.



Figure 3.2 Construction of the rammed stone columns at field

Figure 3.3 shows the special rammer (or tamper) located at the base of the vibroprobe. While raising the pipe, the rammer is opened by gravity and crushed stone is cast in to the driven hole. Afterwards, the pipe is pushed downwards by vertical vibration about 60 cm to compress the crushed stone inside the hole and forces it to spread horizontally into the surrounding soil.



Figure 3.3 Tamper at the tip of the drill rig

### **3.3 Determination of the engineering properties of rammed stone columns**

Information regarding earlier experimental studies available in the literature was used as a guide for the estimation of mechanical properties of stone columns. Internal friction angle of the constructed columns are estimated from the past studies mentioned in Section 2.4.1. In addition to the available data from the previous studies in literature, engineering properties of the rammed stone columns are estimated based on the sieve analysis and single column load tests.

#### **3.3.1 Sieve analysis**

The aggregate used for the rammed stone column element consisted of poorly graded gravel in accordance with TS 1500/2000 soil classification system. Figure 3.4 and Table 3.2 show grain size distribution of the rammed aggregate column material.

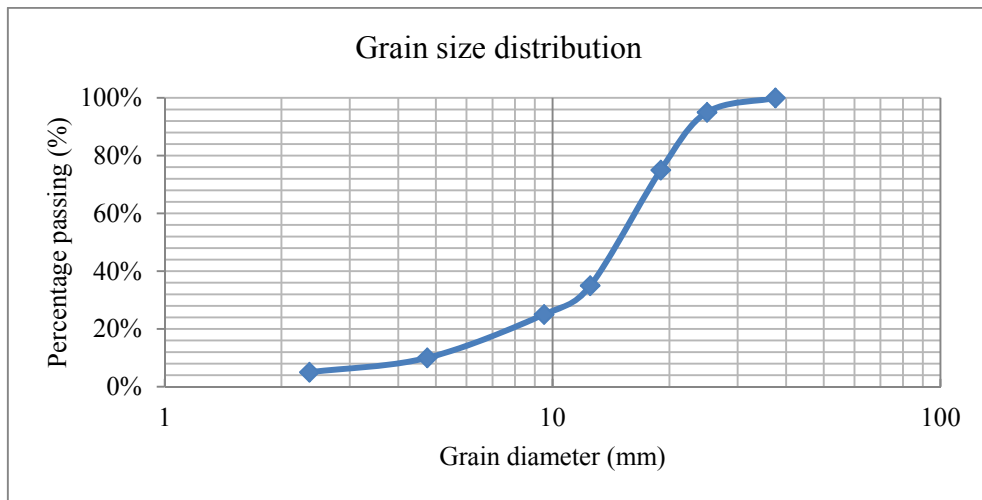


Figure 3.4 Grain size distribution of the aggregate used for the construction of the columns

Table 3.2 Sieve analysis results of the rammed stone column material

Description	Percent passing (%)	Grain diameter (mm)
Coarse gravel	100	37.5
	95	25
	75	19
Fine gravel	35	12.5
	25	9.5
	10	4.75
Coarse sand	5	2.36

### 3.3.2 Evaluation of modulus of subgrade reaction for single rammed stone column

In order to evaluate the modulus of subgrade reaction for single rammed stone column, a test set up, which consisted of a single isolated column, two uplift piles and a reaction frame was constructed. A steel plate with a diameter of the single column is placed on top of the constructed column to apply the load. The test set-up is shown in Figure 3.5. Bulging failure of the rammed stone column which is estimated to be critical, is calculated to occur approximately under a stress of 435 kPa. Load increments to be applied for the single column load test were calculated accordingly based on bulging failure. Applied load increments and related settlement readings are summarized in Table 3.3. Due to economical limitations, telltales could not be used to read the settlements. Thus, the total length of the column is accepted as the length of the constructed column and  $\Delta L$  is accepted to be equal to the settlement readings at the top of the column.



Figure 3.5 Set up of the single rammed stone column test

Table 3.3 Settlement records from the load test of a single column

Percentage of design load (%)	Applied stress (kPa)	Recorded settlement (cm)
25	108.63	0.63
50	217.26	1.29
75	325.9	2.74
100	434.53	3.95
150	651.8	6.55
200	869.06	8.6

Figure 3.6 presents recorded load-settlement plot of the load test for single rammed stone column. The subgrade modulus of the rammed stone column is estimated from the stress-settlement curve of the single column load test presented in Figure 3.6 .

$$k_g = \frac{217.26}{0.0129} = 16842 \frac{\text{kN}}{\text{m}^3}$$

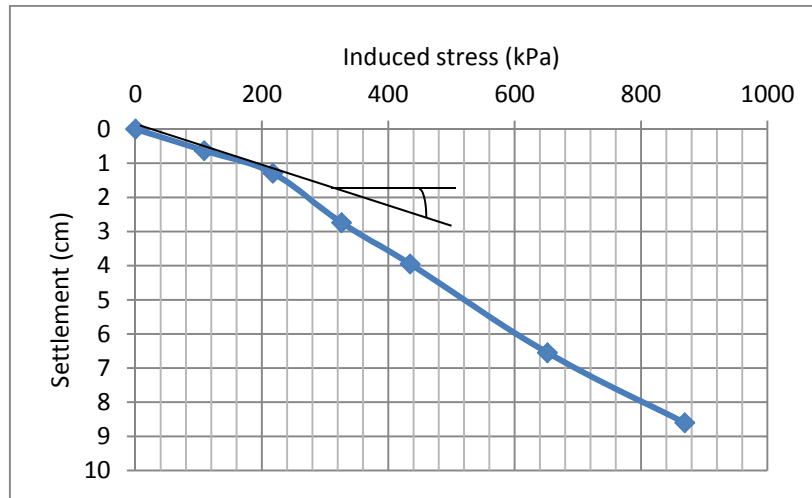


Figure 3.6 Induced stress versus measured settlement from single column load test

Axial strain of the rammed stone column is:

$$\epsilon_g = \frac{\Delta L}{L} \quad (3.1)$$

where,

$\epsilon_g$ : rammed stone column strain

$L_g$ : length of rammed stone column

$\Delta L$ : measured deflection during loading

Using Equation 3.1, strain is calculated as follows:

$$\epsilon_g = \frac{1.29}{510} = 2.53 \times 10^{-3}$$

Subgrade modulus ( $k_g$ ) of the single column is estimated from the load-settlement curve. Up to a settlement of 1.29 cm,  $k_g$  is calculated to be 16842 kPa. Due to the unavailability of telltales, the total length of the column is accepted as the length of the constructed pier and the shortening of the column at each loading step ( $\Delta L_i$ ), expressed in Equation 2.38, is accepted as the settlement readings at the top of the pier.

From Hook's law:

$$\sigma = E_g \times \epsilon_g \quad (3.2)$$

where,

$\sigma$ : stress acting

$E_g$ : elastic modulus of the column

Elastic modulus of the column is calculated using Equation 2.38.

$$E_g = \frac{217.26}{2.53 \times 10^{-3}} \approx 85873 \text{ kPa}$$

Oedometer modulus of the column is calculated as follows.

$$E_{\text{oed},g} = \frac{(1 - \nu)E_g}{(1 - 2\nu)(1 + \nu)} \quad (3.3)$$

$\nu$ : Poisson ratio

$E_g$ : elastic modulus of rammed stone column column

$E_{\text{oed},g}$ : oedometer modulus of rammed stone column material

From Equation 3.3 the oedometer modulus is calculated as follows:

$$E_{\text{oed},g} = \frac{(1 - 0.25) \times 85873}{(1 - 0.5) \times (1 + 0.25)} = 103048 \text{ kPa}$$

Table 3.4 presents the evaluated and predicted rammed stone column material properties.

Table 3.4 Rammed stone column parameters

Property	Value
dry unit weight, $\gamma'_g$ (kN/m <sup>3</sup> )	21
wet unit weight, $\gamma_g$ (kN/m <sup>3</sup> )	23
oedometer modulus, $E_{\text{oed},g}$ (kPa)	103048
modulus of elasticity, $E_g$ (kPa)	85873
Poisson ratio, $\nu$	0,25
effective cohesion, $c'_g$ (kPa)	0
undrained cohesion, $c_{u,g}$ (kPa)	0
effective internal friction angle, $\phi'_g$	45
stiffness, $k_g$ (kN/m <sup>3</sup> )	16842

### 3.4 Bearing capacity calculations of reinforced soil

Before performing the group plate load test on field, bearing capacity and settlement calculations are carried out and pressure to be applied for the plate load test is evaluated. Considering the relevant load-settlement range, nominal length of the column, which is described as the penetration depth of the vibroprobe, is selected as 4.50 m. Pertinent dimensions of the group plate load test setup are provided in Table 3.5.

The unit cell concept is ignored in the group test, because in that approach it is assumed that the columns installed are repeated infinitely in the lateral directions. Whereas in the group load test only four rammed stone columns are constructed.

Table 3.5 Dimensions of the group plate load test setup

Property	Value
nominal diameter of constructed column, d (m)	0.60
shaft diameter of the column, $d_{\text{shaft}}$ (m)	0.676
nominal length of constructed column, $H_0$ (m)	4.50
center to center spacing between column, $s_g$ (m)	1.10
number of constructed columns below cap	4
footing width, B (m)	3.10
footing length, L (m)	3.10
depth of footing below adjacent soil surface (m)	0.40

$$H_0 = 4.50 \text{ m}$$

$d_{\text{shaft}}$  is calculated using Equation 2.8:

$$d_{\text{shaft}} = 0.60 + 0.076 = 0.676 \text{ m}$$

The upper and lower zone depths, which are previously presented in Figure 2.10 are calculated using Equations 2.25 and Equation 2.26, respectively.

$$H_{\text{uz}} = H_{\text{shaft}} = H_0 + d_{\text{shaft}} = 4.50 + 0.676 = 5.176 \text{ m}$$

$$H_{\text{lz}} = 2B - H_{\text{shaft}} = 2 \times 3.10 - 5.176 = 1.02 \text{ m}$$

Area of foundation:

$$A_{\text{foundation}} = 3.10 \times 3.10 = 9.61 \text{ m}^2$$

Area of rammed stone columns:

$$A_{\text{column}} = 4 \times \frac{\pi \times 0.60^2}{4} = 1.13 \text{ m}^2$$

### 3.4.1 Bulging failure of individual rammed stone columns

This section evaluates the failure of a single rammed stone column due to the bulging, the depth of which is calculated using Equation 2.7.

$$z_b = 0.40 + \frac{1}{2} \times 0.60 \times \tan\left(45 + \frac{45}{2}\right) = 1.124 \text{ m}$$

Coefficient of passive earth pressure of the rammed stone column is:

$$K_{p,g} = \tan^2\left(45 + \frac{\phi_g}{2}\right) = \tan^2\left(45 + \frac{45}{2}\right) = 5.828$$

Coefficient of passive earth pressure of the surrounding soil is:

$$K_p = \tan^2\left(45 + \frac{\phi_s}{2}\right) = \tan^2\left(45 + \frac{25}{2}\right) = 2.464$$

Initial vertical effective stress at calculated depth, where bulging failure will occur:

$$\sigma'_{vo} = z_b \times \gamma'_s = 1.124 \times 17.50 = 19.67 \text{ kPa}$$

Total radial stress at the calculated depth, where bulging failure will occur is calculated using Equation 2.1.

$$\sigma_{ro} = \sigma'_{vo} K_p + u_0 = 19.67 \times 2.464 = 48.47 \text{ kPa}$$

Limiting radial stress at calculated depth, where bulging failure will occur is calculated using Equation 2.2.

$$\sigma_{r,lim} = \sigma_{ro} + c_u \left( \ln \frac{E_s}{2c_u(1+v)} \right) = 48.47 + 48 \left( \ln \frac{4800}{2 \times 48 \times (1 + 0.30)} \right) = 223.65 \text{ kPa}$$

Ultimate bearing pressure of single isolated rammed stone column is calculated using Equation 2.3.

$$q_{ult} = \sigma_{r,lim} K_{p,g} = \sigma_{r,lim} \tan^2 \left( 45 + \frac{\phi_g}{2} \right) = 223.65 \tan^2 \left( 45 + \frac{45}{2} \right) = 1303.58 \text{ kPa}$$

### 3.4.2 Shearing failure below tips of individual rammed stone columns

Failure of individual columns due to shearing below tips is evaluated in this section. Applied load on the column is resisted by the shaft and tip resistances of the column as given by Equation 2.9.

$$Q_{tot} = Q_{shaft} + Q_{tip}$$

The equation can be rewritten from Equation 2.10:

$$q_{ult} = f_s \frac{A_{shaft}}{A_g} + q_{tip} = 4 \frac{f_s d_{shaft} H_{shaft}}{d^2} + q_{tip}$$

Vertical effective stress at the middle of the column shaft is calculated as follows:

$$\sigma'_{v,avg} = \left( d_f + \frac{H_{shaft}}{2} \right) \gamma'_s$$

where,

$\sigma'_{v,avg}$ : effective vertical stress at the midpoint of the shaft length

$d_f$ : depth of foundation to the ground surface

$\gamma'_s$ : effective unit weight of the soil

Distance from the center of the column to the surface is calculated below in order to evaluate the effective stress at midpoint of the shaft:

$$d_f + \frac{H_{shaft}}{2} = 0.40 + \frac{5.176}{2} = 2.99 \text{ m}$$

Effective vertical stress at midpoint of the shaft length:

$$\sigma'_{v,avg} = (d_f + \frac{H_{shaft}}{2})\gamma'_s = \left(0.40 + \frac{5.176}{2}\right) \times 17.50 = 52.29 \text{ kPa}$$

Rankine passive earth pressure coefficient:

$$K_p = \tan^2\left(45 + \frac{\phi'_s}{2}\right) = \tan^2\left(45 + \frac{25}{2}\right) = 2.464$$

$$\tan \phi'_s = \tan 25 = 0.47$$

Average unit friction along shaft is calculated using equation 2.14.

$$f_s = \sigma'_{v,avg} K_p \tan(\phi'_s) = 52.29 \times 2.464 \times 0.47 = 60.56 \text{ kPa}$$

Overburden stress at the elevation of the tip of column is:

$$\sigma'_{v,tip} = 5.176 \times 17.50 = 90.58 \text{ kPa}$$

Tip resistance of the column is calculated using Equation 2.16.

$$q_{tip} = cN_c + \frac{1}{2}d_{shaft}\gamma_s N_\gamma + \sigma'_{v,tip} N_q = 8 \times 25.1 + 0.50 \times 0.676 \times 17.50 \times 9.7 + 90.58 \times 9.7 = 1136.80 \text{ kPa}$$

Hence, the total ultimate bearing pressure is calculated by Equation 2.10.

$$q_{ult} = 4 \frac{f_s d_{shaft} H_{shaft}}{d^2} + q_{tip} = 4 \times \frac{60.56 \times 0.676 \times 5.176}{0.60^2} + 1136.80 = 3491.22 \text{ kPa}$$

### 3.4.3 Shearing failure within the reinforced soil zone

Shearing failure within reinforced soil matrix is studied in this section.

Stress concentration ratio, which is defined as the ratio of the stress acting on the column to the stress acting on the surrounding soil, is determined based on Wiessmann's (1999) recommendations and previous studies provided in literature and summarized in Table 2.1.

$$n = 2.8$$

Area replacement ratio is calculated as the ratio of the area of columns in the group to the gross area of the soil matrix.

$$R_a = \frac{A_g}{A} = \frac{1.13}{9.61} = 0.117$$

As it is previously explained in section 2.2.1, the area replacement ratio is multiplied by a reduction factor of 0.4 using Equation 2.19.

$$R'_a = 0.40 \times 0.117 = 0.05$$

Composite shear strength parameters are calculated as follows, using Equation 2.17 and Equation 2.18 respectively.

$$\phi_{comp} = \tan^{-1}[0.05 \times 2.8 \times \tan 45 + (1 - 0.05 \times 2.8) \tan 25] = 28^\circ$$

$$c_{\text{comp}} = (1 - 0.05 \times 2.8) \times 8 = 6.7 \text{ kPa}$$

Bearing capacity factors:

$$N_c = 31.61$$

$$N_q = 17.81$$

$$N_y = 15.15$$

Foundation shape factors for square foundation:

$$s_c = 1.3$$

$$s_y = 0.8$$

Ultimate bearing pressure is calculated using Equation 2.42.

$$q_{\text{ult}} = 6.70 \times 31.61 \times 1.3 + 0.40 \times 17.50 \times 17.81 + 0.5 \times 17.50 \times 3.10 \times 15.15 \times 0.8 = 728.75 \text{ kPa}$$

#### 3.4.4 Shearing failure below the reinforced soil zone

In this section, ultimate bearing pressure for the shearing failure below reinforced soil matrix is evaluated.

Overburden stress at the elevation of the tip of column is calculated as follows:

$$\sigma'_{v,\text{tip}} = 5.176 \times 17.50 = 90.58 \text{ kPa}$$

Footing ultimate bearing pressure at the bottom of the reinforced soil is calculated using Equation 2.42:

$$q_{\text{bottom}} = 6.70 \times 25.225 \times 1.3 + 5.176 \times 17.50 \times 12.805 + 0.5 \times 17.50 \times 3.10 \times 6.61 \times 0.8 = 1523.02 \text{ kPa}$$

Ultimate bearing pressure for the shearing below reinforced soil matrix is calculated through Equation 2.22.

$$q_{\text{ult}} = q_{\text{bottom}} \times \frac{(B + H_{UZ})(L + H_{UZ})}{BL} = 1523.02 \times \frac{(3.10 + 5.176) \times (3.10 + 5.176)}{3.10 \times 3.10} = 10854.83 \text{ kPa}$$

Result of each bearing capacity calculation of the reinforced soil corresponding to a specific failure mechanism and given above in detail is listed in Table 3.6.

Table 3.6 Failure mechanism and respective bearing capacity of the reinforced soil

Failure mechanism	Ultimate bearing pressure (kPa)	Allowable bearing capacity (kPa)	Factor of safety
Bulging failure of individual columns	1303	435	3
Shearing failure below tips of individual columns	3491	1164	
Shearing failure within reinforced soil zone	729	243	
Shearing failure below reinforced soil zone	10855	3618	

Ultimate capacity has been calculated based on the results given in Table 3.5. When considering the reinforced soil as a whole, the most critical failure mechanism appears to be due to the shearing within the reinforced soil. Taking this into consideration, stress on each rammed stone column at ultimate capacity is calculated using Equation 2.31.

$$q_g = \frac{q_0 n}{R_a(n-1) + 1} = \frac{242.92 \times 2.8}{0.117 \times (2.8 - 1) + 1} = 561.85 \text{ kPa}$$

The calculated value above exceeds the limit of bulging failure of a column, which is shown in Table 3.5 to be 434.53 kPa. Ultimate bearing pressure is then, re-calculated for that reason by taking into consideration the bulging failure of individual columns.

$$q_0 = \frac{q_g(R_a(n-1) + 1)}{n} = \frac{434.53 \times (0.117 \times (2.8 - 1) + 1)}{2.8} = 188 \text{ kPa}$$

Applying the factor of safety of three, the design load is:

$$q_0 = 188 \times 3 = 564 \text{ kPa}$$

### 3.5 Settlement calculations of reinforced soil

Settlements from primary and secondary consolidation of the lower zone are ignored due to fast loading speed of the plate load test on field. Settlement calculations are made using Equation 2.23.

$$s_{\text{tot}} = s_{i,uz} + s_{i,lz}$$

Total stress acting on reinforced soil is calculated as the sum of the load transferred from the superstructure and self-weight of the foundation. Pressure due to the foundation weight which will act on the soil is calculated:

$$q_{\text{foundation}} = 24 \times 0.4 = 10 \text{ kPa}$$

$$q_0 = q_{\text{applied stress}} + q_{\text{foundation}} = 188 + 10 = 198 \text{ kPa}$$

### 3.5.1 Immediate settlement of the upper zone

Stress acting on the rammed stone column under an applied stress is calculated using Equation 2.31.

$$q_g = \frac{q_0 n}{R_a(n-1) + 1} = \frac{(198) \times 2.8}{0.117 \times (2.8 - 1) + 1} = 457.95 \text{ kPa}$$

Immediate settlement of the upper (reinforced) soil layer is calculated using Equation 2.33.

$$s_{i,uz} = \frac{q_g}{k_g} = \frac{457.95}{16482} = 0.0272 \text{ m}$$

### 3.5.2 Immediate settlement of the lower zone

Dimensions provided in Table 3.5, and illustrated in Figures 2.10 and 3.1, relating to the group load test are utilized for the elastic settlement calculations.

$$H_0 = 4.50 \text{ m}$$

$$d = 0.60 \text{ m}$$

$$d_{\text{shaft}} = 0.676 \text{ m}$$

$$H_{uz} = 5.176 \text{ m}$$

$$H_{lz} = 1.02 \text{ m}$$

$$\frac{D}{B} = 1.798$$

$$\frac{H}{B} = 0.33$$

$A_1$  and  $A_2$  are selected from Figure 2.12.

$$A_1 = 0.08$$

$$A_2 = 0.90$$

Settlement of the lower zone is calculated using Equation 2.36.

$$s_{lz} = 0.08 \times 0.90 \times \frac{198 \times 3.1}{4800} = 0.0092 \text{ m}$$

Overall total settlement is the sum of the settlements of lower and upper zones.

$$s_{\text{tot}} = s_{uz} + s_{lz} = 2.72 + 0.92 = 3.69 \text{ cm}$$

Table 3.7 summarizes elastic settlement calculations exposed to different stresses.

Table 3.7 Elastic settlement calculations

Percentage of design load (%)	Foundation pressure (kPa)	Elastic settlement of the upper zone (cm)	Elastic settlement of the lower zone (cm)	Total elastic settlement (cm)
25	57	0.78	0.26	1.04
50	104	1.43	0.48	1.91
75	151	2.07	0.70	2.77
100	198	2.72	0.92	3.64
125	245	3.36	1.14	4.50
150	292	4.01	1.36	5.37
200	386	5.3	1.79	7.09

### 3.6 Plate load test on a group of rammed stone columns

A picture of the group load test setup is presented in Figure 3.7. Four rammed stone columns are constructed with a reinforced concrete cap. Four tension piles are considered to be sufficient to provide the adequate reaction. A lever jack is used with a maximum loading capacity of 800 tons. Complete jacking system is calibrated before the beginning of the test. The hydraulic jack is placed at the center of the cap so that the loads are applied concentrically to the cap. The 40 cm thick cap is deemed to distribute the applied load uniformly to the ground. For each load increment, settlement readings were recorded by two gauges. ASTM D 1143-81 standard is followed in preparation of the test setup and during the load application stage.



Figure 3.7 A view of the group load test setup

In the first half an hour of the test, readings are taken at intervals not exceeding 10 min. Then, each load increment maintained until the rate of settlement becomes less than 0.25 mm/h but not longer than 2 h. During unloading, readings were taken at intervals not exceeding 20 min. A final rebound reading is taken 12 h after all loads have been removed. Figure 3.8 and Table 3.8 present each step of load settlement readings recorded during the test.

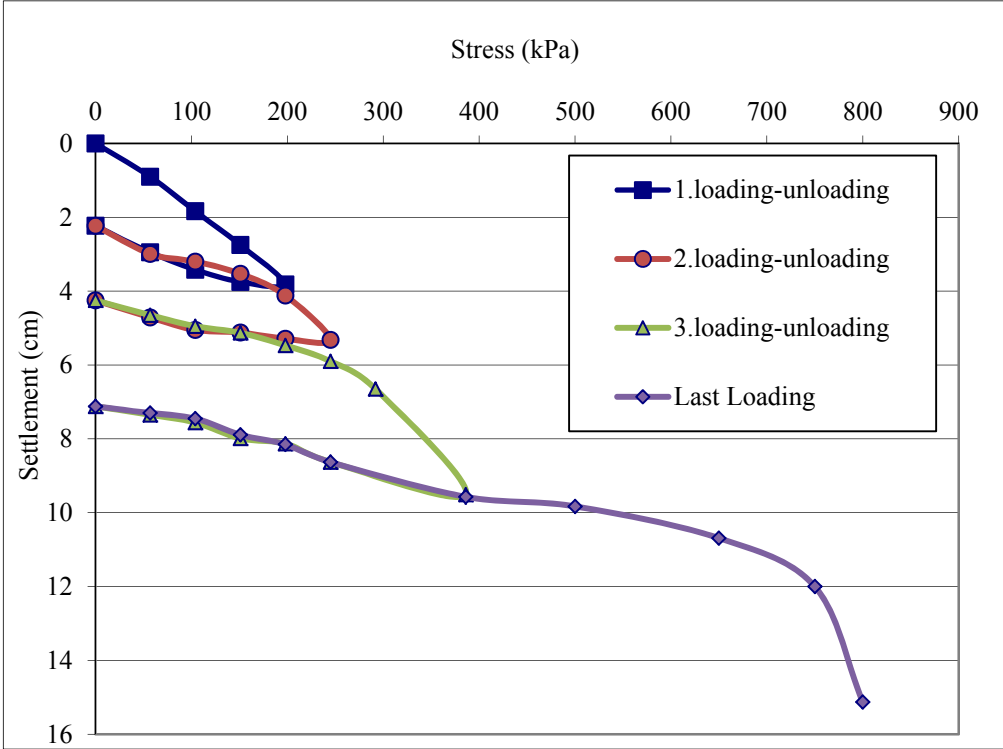


Figure 3.8 Load-settlement plot recorded during group load test

Table 3.8 Settlement records of the group load test

Percentage of design load (%)	Foundation pressure (kPa)	Recorded pile head displacement (cm)
25	57	0.9
50	104	1.84
75	151	2.75
100	198	3.82
125	245	5.32
150	292	6.65
200	386	9.51

Table 3.9 shows recorded settlements after each loading and unloading sequence. It is assumed that the difference between recorded pile head displacement at examined stress and displacement after unloading reveals the elastic settlement.

Table 3.9 Settlement readings from loading-unloading curve of the plate load test on group of columns

Load step	Loading type	Percentage of design load (%)	Foundation pressure (kPa)	Recorded pile head displacement (cm)	Elastic settlement at load step (cm)
1	Loading	75	151	2.75	0.52
	Unloading	0	0	2.23	
2	Loading	125	245	5.32	1.07
	Unloading	0	0	4.25	
3	Loading	200	386	9.51	2.39
	Unloading	0	0	7.12	

### 3.6.1 Determination of ultimate bearing capacity from stress-settlement data

Ultimate bearing capacity of a rammed stone column reinforced soil is estimated using different methods applied to full scale field test results in order to compare with the ultimate bearing capacity calculations of reinforced soil. Calculation technicalities involving relevant graphs are given in Appendix B. Capacity of a rammed stone column group can be calculated using methods that are developed for and commonly applied to piles. Accordingly, Chin Kondner, Decourt's extrapolation and Mazurkiewicz's methods are used to estimate the bearing capacity of the reinforced soil and the calculated values are compared to the most critical failure stresses in Table 3.10.

Table 3.10 Comparison of ultimate bearing capacity results of different methods

Method of calculation	Evaluated ultimate bearing pressure of reinforced soil (kPa)
Limit equilibrium theory (Shearing within reinforced soil zone)	729
Chin-Kondner method	1000
Decourt's extrapolation method	944
Mazurkiewicz's method	950
Observed ultimate capacity from load test	800

### 3.6.2 Comparison of settlements from single and group rammed stone column tests

Figure 3.9 presents the load-settlement curve of the single loaded column and that of group of rammed stone columns. The line which represents the group of loaded columns considers the stress acting on the column as a result of applied total stress. Table 3.11 presents calculated values of stresses acting on rammed stone columns using stress concentration ratio,  $n$  and area replacement ratio,  $R_a$  and compares settlement readings from the plate load test on a group of rammed stone column elements and a single rammed stone column load test.

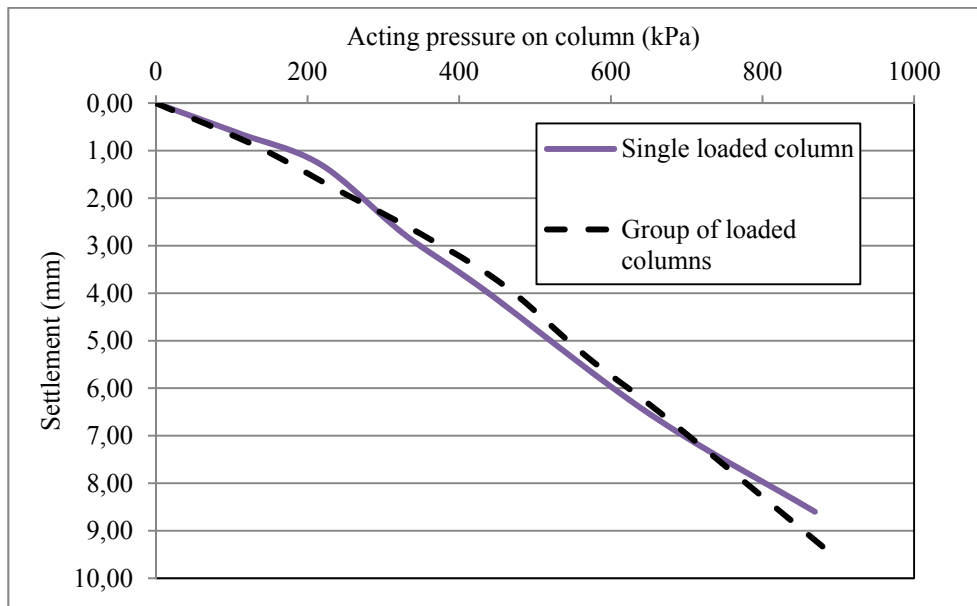


Figure 3.9 Comparison of the stress-displacement plots of a single loaded column and group columns

Table 3.11 Comparison of settlement readings of single loaded column and group of columns

Induced stress (kPa)	Area ratio	Stress ratio	Group of rammed stone column elements		Single rammed stone column element	
			Stress acting on rammed stone columns (kPa)	Measured settlement (cm)	Induced stress (kPa)	Measured settlement (cm)
0			0	0	0	0
57			131.84	0.9	108.63	0.63
104			240.54	1.84	217.26	1.29
151	0.117	2.8	349.25	2.75	325.9	2.74
198			457.95	3.82	434.53	3.95
245			566.67	5.32	651.8	6.55
292			675.37	6.65	869.06	8.6
386			892.78	9.51		

### 3.7 Evaluation of the reinforced model using finite element method

This section consists of the analyses of reinforced soil through finite element method using the software package PLAXIS 3D by the same model and design parameters as in the previous sections which have been used in the ultimate bearing capacity and settlement calculations.

### 3.7.1 General model properties

In the finite element code, the same model is created as that constructed for the group column plate load test in the field. The depth and width of the model are selected as sufficient so that it acquires real behaviour of the model. Standard boundary option is selected in the program. This boundary option models the top surface to be free of movement into all directions. When considering the model boundary in yz-plane, displacements in the x directions are limited to zero where displacements in the y and z directions are free. All boundaries are modelled in the same manner. The bottom boundary is fixed in all directions. It is of important that a suitable mesh size is selected that it is fine enough to capture the real behaviour of the model where therewithal the analysis time does not become unreasonable. Due to that reason the global mesh coarseness is selected in the medium range, in addition, the software automatically refines the critical areas in the model. The created geometry of the model and the generated mesh used in analyses are presented in Figure 3.10 (a) and (b), respectively.

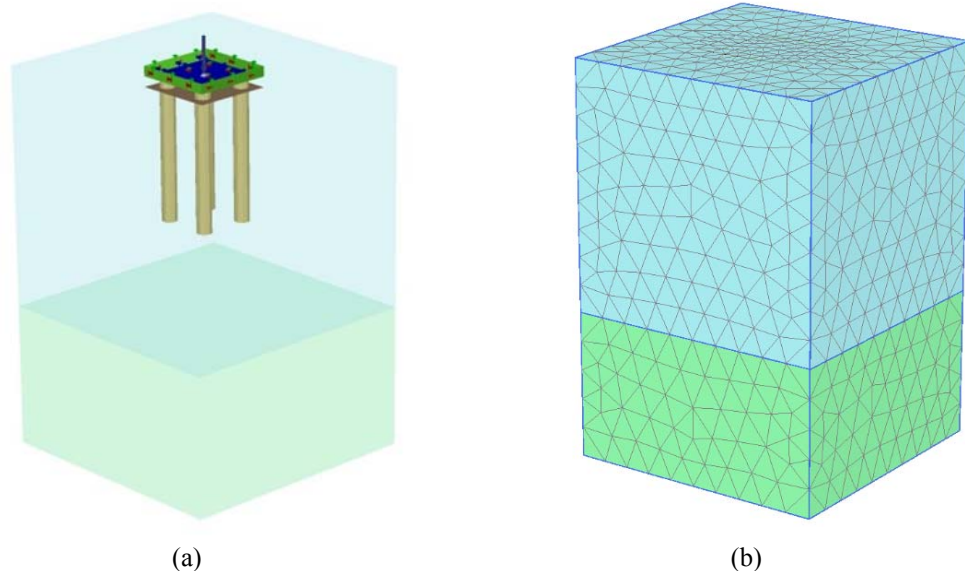


Figure 3.10 (a) Input geometry of the analyzed model in PLAXIS 3D (b) Generated mesh

### 3.7.2 Material properties

Materials of the general soil profile and the rammed stone columns are represented by the linear elastic-perfectly plastic Mohr-Coulomb criteria. The model requires five input parameters: Young's modulus ( $E$ ) as the basic stiffness parameter, Poisson's ratio ( $\nu$ ), internal friction angle ( $\phi$ ), cohesion ( $c$ ) and dilatancy angle ( $\psi$ ). Since no groundwater is observed within the depth of interest at the site, and since the site soils are unsaturated, drained analysis is preferred in the analyses. A floor element is used to model the pile cap. The floor element is defined by thickness, unit weight and stiffness. Material parameters utilized for soil and rammed stone columns are summarized in Table 3.12.

Table 3.12 Finite element model input parameters

Material property	Material type		Structural elements
	Clay Mohr coulomb - drained	Rammed stone column Mohr coulomb - drained	Pile cap Linear, isotropic
$\gamma$ (kN/m <sup>3</sup> )	-	-	24
$\gamma_{\text{unsat}}$ (kN/m <sup>3</sup> )	17.50	21	-
$\gamma_{\text{sat}}$ (kN/m <sup>3</sup> )	18.50	23	-
$E'$ (kN/m <sup>2</sup> )	4800	85873	3E <sup>7</sup>
$E_{\text{oad}}$ (kN/m <sup>2</sup> )	6461	103048	-
$c'$ (kN/m <sup>2</sup> )	8	0	-
$\phi'$	25	45	-
$\psi$	0	5	-
$\nu'$	0.3	0.25	0.15
$d$ (m)	-	-	0.40

### 3.7.3 Analyses of the model

Following the modeling of the general form of the rammed stone columns and soil layers, the calculation phase is applied with load inputs. The staged construction approach is selected to specify the different load increments. The calculation type chosen is plastic calculation which performs an elastic-plastic deformation analysis. In-situ stresses are calculated in the initial phase. Structural elements have been activated in phase 1. Table 3.13 shows the calculation steps implemented in the finite element code. Displacements are reset to zero following the application of in-situ stress. The loading pattern in the model is defined in different phases in which the assigned point load on the columns is increased to a specific level based on the test standards.

Table 3.13 Calculation steps in the finite element program

Phase	Calculation type	Construction phase
Initial	$K_0$ procedure	Initial stresses
Phase 1		Installation of pile cap
Phase 2		Application of 25% of degin load
Phase 3		Application of 50% of degin load
Phase 4	Plastic analysis	Application of 75% of degin load
Phase 5		Application of 100% of degin load
Phase 6		Application of 125% of degin load
Phase 7		Application of 150% of degin load
Phase 8		Application of 200% of degin load

### 3.7.4 Analyses results

For each stresses applied, the resulting maximum deformation at the foundation is evaluated. Figure 3.11 depicts a cross section which shows vertical deformations under an applied stress of 286 kPa. A summary of settlement results are given in Table 3.14. Settlements evaluated from the finite element analyses are compared to those measured during the group load test at the field and those obtained from empirical correlations. Figure 3.12 shows the pressure - displacement curves resulting from elastic settlement calculations, load test on group of columns and finite element model analyses. Cross sections taken through the x-y plane which are given in Appendix C show the stress concentrations acting on the reinforced soil. It can be obviously seen that stresses acting on columns are higher then the matrix soil.

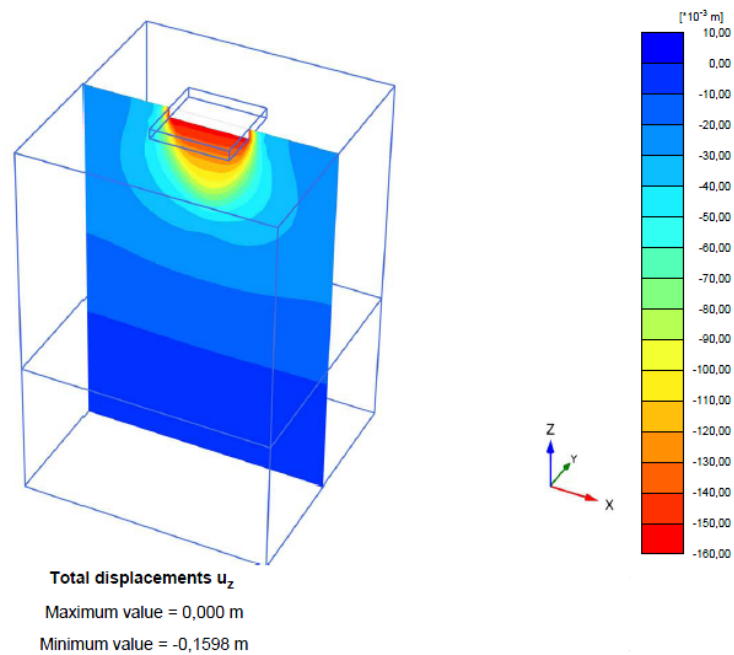


Figure 3.11 Cross section showing settlements at maximum stress step

Table 3.14 Settlements resulting from finite element analyses

Percentage of design stress (%)	Applied foundation pressure (kPa)	Plaxis 3D settlement results (cm)
25	57	1.14
50	104	2.38
75	151	3.91
100	198	5.74
125	245	7.71
150	292	9.71
200	386	15.98

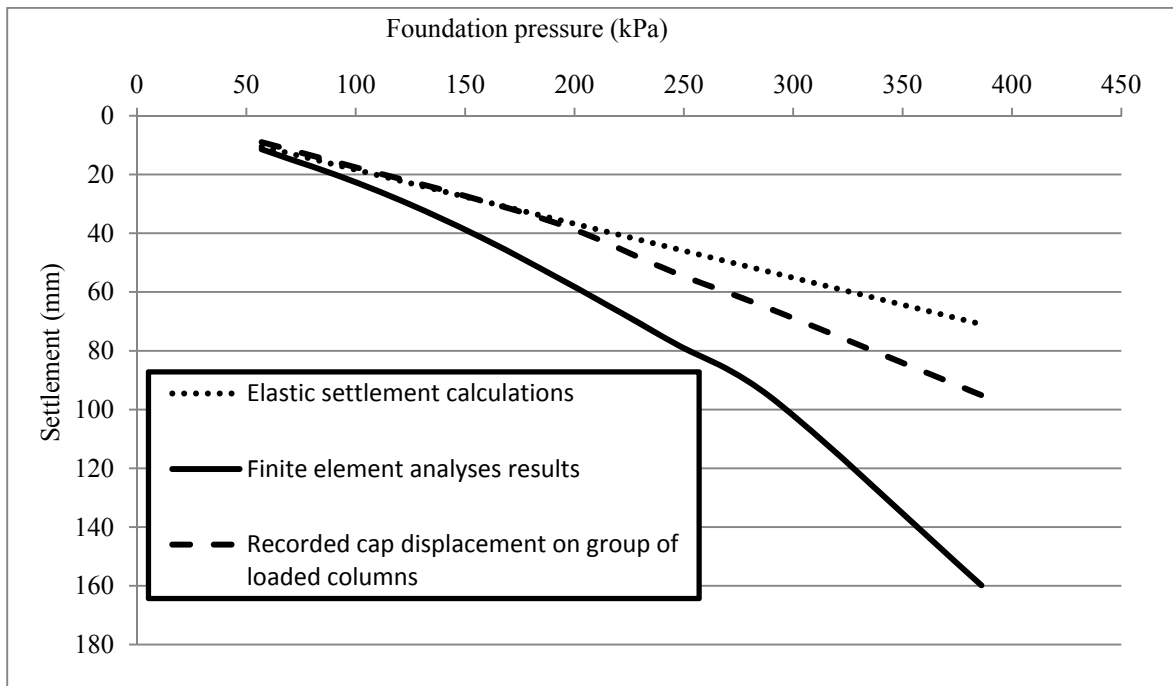


Figure 3.12 Comparison of stress-settlement responses

## CHAPTER 4

### SUMMARY, DISCUSSIONS AND CONCLUSIONS

#### 4.1 Summary

The content of this study can be summarized as follows.

- ✓ Existing design principles for bearing capacity and settlement predictions of rammed stone columns supported footings from the literature are reviewed and evaluated.
- ✓ In order to estimate the relevant parameters of the subsurface profile of investigated site, a number of laboratory and in-situ tests are carried out.
- ✓ A load test is conducted on a single rammed stone column in order to evaluate the response and modulus of subgrade reaction of single rammed stone column.
- ✓ A load test over a group of four closely spaced rammed stone columns with a reinforced concrete cap is conducted.
- ✓ Response of the single column is compared to that of the group of rammed stone columns subjected to vertical loading.
- ✓ Ultimate bearing capacity of the rammed stone column reinforced soil is estimated using different methods based on the field test results of reinforced soil with a group of columns and compared with the calculated results for the same model.
- ✓ Finite element method is utilized to simulate the field load tests with a group of columns.
- ✓ Based on the evaluation of all possible failure mechanisms for the studied case of rammed stone column reinforced soil and individual column, failure within reinforced soil has been considered to be the most critical failure mechanism. However, the stresses acting on a rammed stone column when exposed to that load capacity exceeded the limit for the bulging of a single column. Thus, design is limited by the bulging of a single column.
- ✓ Settlements obtained utilizing empirical equations are compared to those of the group of rammed stone column load test results and finite element analyses. Figure 3.12 presents a comparison of all settlements resulting from different methods.

#### 4.2 Discussions and conclusions

Following statements can be inferred based on the results of this study.

- ✓ Although the Chin-Kondner, Decourt's extrapolation and Mazurkiewicz's methods predict the ultimate bearing capacity from stress-settlement curves reasonably, it can be speculated that all three approximations overestimate the ultimate bearing capacity by 37%, 29% and 30%, respectively, compared to the calculated ultimate bearing capacity of 729 kPa.
- ✓ After three consecutive loading and unloading sequences during loading of the group of rammed stone columns, the load has been increased until failure. The failure of the reinforced

soil from the plate load test is defined as the respective point on the curve where the curvature of the stress-settlement curve approaches to zero, which approximately corresponds to 800 kPa. This value is well above the bulging limit of an individual column, which is 564 kPa; but close to the shearing capacity of 729 kPa of the reinforced soil. When designing for a group of columns, the consideration of the failure of a single column would be too conservative, where even the bearing capacity estimations of rammed stone column groups are stated to be underestimated in the literature. The same trend is also observed in this study.

- ✓ It can be said from settlement results shown in Table 4.1 that within 50% of the design stress, calculated elastic settlements, finite element analyses results and plate load test records agree quite well with each other. However, with the increase of applied stress, particularly when it exceeds the allowable bearing capacity, the plastic failures seem to become prominent. This can be observed from the differences between calculated and recorded elastic settlements and in-situ test results.
- ✓ Settlement results from the finite element analyses compared to settlement records of the plate load test seem to yield reasonably comparable values up to 50% of the design load. Afterwards, the recorded settlements display up to 42% lower values compared to the finite element analyses results, and the difference mounts up to 68% under 200% of the design stress. This observation can be attributed to the occurrence of plastic failures under increasing demand, following an initial elastic response.
- ✓ Elastic settlements recorded from the load test on group of columns are presented in Table 3.9. When these values are compared to those calculated, major differences are observed. These differences can be attributed to the following reasons: Elastic settlements are basically dependent upon the modulus of elasticity of the soil and the modulus of subgrade reaction of the rammed stone column. Young's modulus of the soil is assessed based on pressuremeter tests, whereas the modulus of subgrade reaction of the rammed stone column is obtained from plate load test on single column. Accordingly, differences may occur due to the small discrepancies in the geological formations. On the other hand, the elastic settlement calculation of the rammed stone column is basically dependent on the stress concentration ratio which is selected based on the past studies. This ratio might also be effective on elastic settlement differences.
- ✓ Results shown in Figure 3.9 indicate that the group of columns tend to settle less even if just a small amount, when compared to single column under a given stress. This may be attributed to the tendency of a column to bulge under applied vertical stress, which in turn compresses and strengthens the matrix soil. It is to be noted that the compaction of the matrix soil would be more pronounced in the case of group of columns. However, the small settlement difference observed can be explained to be due to that reason that no surrounding columns were installed around the group of four columns. Stiffer matrix soil decreases the total settlement amount. With increasing stress (after 700 kPa), single column tends to settle less which referred in previous studies as the negative group effect (Lawton, 2004).
- ✓ Results show that reinforcing of the weak soils using rammed stone columns is an effective way of increasing soil stiffness and strength. The results show that in most of the practical footing design cases, the allowable bearing pressure should be controlled by settlement rather than the ultimate capacity. Due to that reason, the settlement predictions are recommended to be made scrupulously.
- ✓ The methods currently used in practice to predict settlement and bearing capacity of reinforced soil constructed using rammed stone columns seem to be capable with sufficient precision. Finite element analyses results and field group tests seem to give reliable results when assuming the strength parameters of the soil carefully.

## REFERENCES

- Abdelrahman, G.E., Shaarawi, E.M., and Abouzaid K.S. (2003). "Interpretation of axial pile load test results for continuous flight auger piles" Proc. Of the 9<sup>th</sup> Arab Structural En. Conf.
- Aboshi, H., Ichimoto, E., Enoki, M. and Haraka, K. (1979), "The Compozer – A Method to Improve Characteristics of Soft Clays by Inclusion of Large Diameter Sand Columns". Proceedings of International Conference on Soil Reinforcement: Reinforced Earth and other Techniques, Paris, Vol. 1, p.211-216.
- American Society for testing and material, (1994), "D 1143-81 Standard Test Method for Piles Under Static Axial Compressive Load"
- Barksdale, R. D., and Bachus, R. C. (1983). "Design and construction of stone columns: Vol. 1," Report No. FHWA/RD-83/026, U.S. Department of Transportation, Federal Highway Administration.
- Bowles, J. E. (1996). Foundation Analysis and Design, 5th ed., McGraw-Hill, New York.
- Brown, R. E. and Glenn, A. J. (1976). "Vibroflotation and Terra-Probe Comparison", Journal of Geotechnical Engineering Division, ASCE, 102(GT10), 1059-1072.
- Brown, R. E. (1977). "Vibroflotation Compaction of Cohesionless Soils", Journal of Geotechnical Engineering Division, ASCE, 103(GT12), 1437-1450.
- Chin, F.K. (1970). "Estimation of the Ultimate Load of Piles not carried to Failure. Proceedings of the 2<sup>nd</sup> Southeast Asian Conference ON Soil Engineering, 81-90"
- Chin, F.K. (1971). "Discussion of Pile Test ", Arkansas River Project, Journal for Soil Mechanics and Foundation Engineering, ASCE, vo. 97, SM 6, 930-932
- Christian, J. T., Carrier III, W. D. (1978). "Janbu, Bjerrum and Kjaernsli's chart reinterpreted." Canadian Geotechnical Journal, 15 (1), 123 - 128
- Das, B. M. (1997). Advanced Soil Mechanics, 2nd ed., Taylor and Francis, New York.
- Decourt, L. (1999). "Behavior of foundations under working load conditions", Proceedings of the Pan-American Conference on Soil Mechanics and Geotechnical Engineering, Foz Dolguassu, Brazil, August 1999, Vol. 4, pp. 453-488
- Federal Highway Administration Reports (1983), "Design and construction of stone columns", Vol.1 Report o. FHWA/RD-83/026
- Fox, N. S., and Lawton, E. C. (1993). "Short aggregate piers and method and apparatus for producing same." U.S. Patent No. 5,249,892, issued October 5.
- Fox, N. S., and Cowell, M. J. (1998). Geopier Foundation and Soil Reinforcement Manual, Geopier Foundation Co., Inc., Scottsdale, Arizona, September.
- Gaul, A. J. (2001). "Embankment Foundation Reinforcement using Rammed Aggregate Piers in Iowa Soils", MS thesis, Department of Civil and Environmental Engineering, Iowa State University, Ames, Iowa, 154 pp.
- Gibson, R. E. and Anderson, W. F. (1961). "In situ measurements of soil properties with the pressuremeter." Civil Engineering and Public Works Review, Vol. 56, No. 658.

- Hayward Baker Inc. (1996). "Ground Modification Seminar Notes", Hayward Baker, Odenton, Maryland, 102pp.
- Handy, R. L., and Fox, N. S. (1967). "A Soil Borehole Direct-Shear Test Device." Highway Research News, Vol. 27, pp. 42-51.
- Handy, R. L. (1985). "The Arch in Soil Arching." Journal of Geotechnical Engineering, ASCE, Vol. 111, No. 3, pp. 302-318.
- Hughes, J. M., and Withers, N. J. (1974). "Reinforcing of soft cohesive soils with stone columns." Ground Engineering, May 1974, pp. 42-49.
- Hughes, J. M. O., Withers, N. J. and Greenwood, D. A. (1975). "A field trial of the reinforcing effects of a stone column in soil." Geotechnique, Vol. 25, pp. 31-44.
- Lambe, T. W., and Whitman, R. V. (1969). Soil Mechanics: SI Version, John Wiley and Sons, New York.
- Lawton, E. C., N. S., and Handy, R. L. (1994). "Control of settlement and uplift of structures using short aggregate piers." In-Situ Deep Soil Improvement, ASCE Geotechnical Special Publication No. 45, pp. 121-132
- Lawton, E. C., and Fox, N. S. (1994). "Settlement of structures supported on marginal or inadequate soils stiffened with short aggregate piers." Vertical and Horizontal Deformations of Foundations and Embankments, ASCE Geotechnical
- Lawton, E. C. (1999). "Performance of Geopier foundations during simulated tests at South Temple bridge on Interstate 15, Salt Lake City, Utah." Interim Report, No. UUCVEEN 99-06, University of Utah, Salt Lake City.
- Lawton, E.C. (2000) "Performance of Geopier-supported foundations during simulated seismic tests on northbound interstate 15 bridge over south temple, salt lake city utah." Final report, Report No. UUCVEEN 04-12, (July 2004): 239 pgs.
- Lawton, E. C. (2001). "Soil improvement and stabilization: Non-grouting techniques." Section 6 in Practical Foundation Engineering Handbook, 2nd ed., Ed. by R. W. Brown, McGraw-Hill, New York, pp. 6.1 - 6.340.
- Lawton, E.C. (2004) "Performance of Geopier elements loaded in compression compared to single Geopier elements supported foundations during simulated seismic tests on northbound interstate 15 bridge over south temple, salt lake city utah." Final Report, Report No. UUCVEEN 00-03, the University of Utah, (December 2000): 73 pgs.
- Lopez, R. A. and Hayden, R. F. (1992). "The Use of Vibro Systems in Seismic Design", Grouting, Soil Improvement and Geosynthetics, Borden, R. H., Holtz, R. D., and Juran, I., eds., Geotechnical Special Publication No. 30, ASCE, 2, 1433-1445.
- Mazurkiewicz, B.K. (1972). "Test loading of piles according to Polish regulations", Royal Sw. Acad. of Engng. Sciences, Conn. On Pile Research, Report No. 35, Stockholm 20 pp.
- Meyerhof, G.G. (1963) "Some recent research on the bearing capacity of foundations" Canadian Geotechnical Journal, Vol.1, pp. 16-31.
- Mitchell, J.K., (1981), "Soil Improvement: State-of-the-Art Report," Session 12, Tenth International Conference on Soil Mechanics and Foundation Engineering, Stockholm, Sweden, June 15-19.

- Munfakh, G. A., Abramson, L. W., Barksdale, R. D., and Juran, I. (1987). "In-Situ Ground Reinforcement", Soil Improvement – A Ten Year Update, Welsh, J. P., ed., Geotechnical Special Publication No. 12, ASCE, 1-17.
- Priebe, H. J. (1978), "Abschaetzung des Scherwiderstandes eines durch Stopfverdichtung verbesserten Baugrundes," Die Bautechnik, (55), 8, 281-284.
- Priebe, H. J. (1995) "The design of vibro replacement" Technical paper GT 07-13 E
- Razeghi, H. R. (2011) "Comparison of experimental and analytical results in rammed aggregate piers with variable diameters" Transportation research journal vol. 1 pg. 75-86
- Saito, A. (1977). "Characteristics of Penetration Resistance of a Reclaimed Sandy Deposit and Their Change through Vibratory Compaction", Soils and Foundations, 17(4), 31-43.
- Skempton, A. W. (1957). "The pore-pressure coefficients A and B," Geotechnique, Vol. 14, No. 2, pp. 77-101.
- Skempton, A. W. and Bjerrum, L. (1957), "A contribution to the settlement analysis of foundations on clay," Geotechnique, Vol. 7, No. 4, pp. 168-178.
- Suleiman, M. T., White, D. J. (2006) "Load Transfer in Rammed Aggregate Piers", International Journal of Geomechanics, Vol. 6, No.6.
- Terzaghi, K. (1943) "Theoretical soil mechanics John Wiley and sons, In., New York"
- Terzaghi, K. (1955). "Evaluation of Coefficients of Subgrade Reaction." Geotechnique, Vol. 5, No. 4, December, pp. 297-326.
- Vesic, A. S. (1972). "Expansion of cavities in infinite soil mass." J. Soil Mech. Found. Div., 98(3), 265–290.
- Vesic, A. S. (1973). "Analysis of ultimate loads of shallow foundations." Journal of the Soil Mechanics and Foundations Division, Vol. 99, No. 1, pp. 45-73.
- Vesic, A. S. (1975). "Bearing capacity of shallow foundations." Section 3 in Foundation Engineering Handbook, Edited by H. F. Winterkorn and H-Y Fang.
- Whire, D.J. (2001). "Letter to Geopier Foundation Company. Iowa State University. November 20, 2001.
- White, D.J., Wissmann, K.J., Barnes, A.G., and Gaul, A.J. (2002). "Embankment Support: A Comparison of Stone Column and Rammed Aggregate Pier Soil Reinforcement." Presented, Transportation Research Board. 81st Meeting, Washington, D.C. January 13-17.
- Wissmann, K. J. (1999). "Bearing capacity of Geopier-supported foundation systems." Technical Bulletin No. 2, Geopier Foundation Co., Inc., Scottsdale, Arizona.
- Wissmann, K. J., Fox, N. S., Martin, J. P. (2000) "Rammed aggregate piers defeat 75-foot long driven piles" Proceedings of the conference American Society of Civil Engineers, Amherst, Massachusetts.
- Wissmann, K.J., FitzPatrick, B.T., White, D.J., and Lien, B.H. (2002). "Improving global stability and controlling settlement with Geopier soil reinforcing elements." Proceedings, 4th International Conference on Ground Improvement. Kuala Lumpur, Malaysia, 26-28 March.

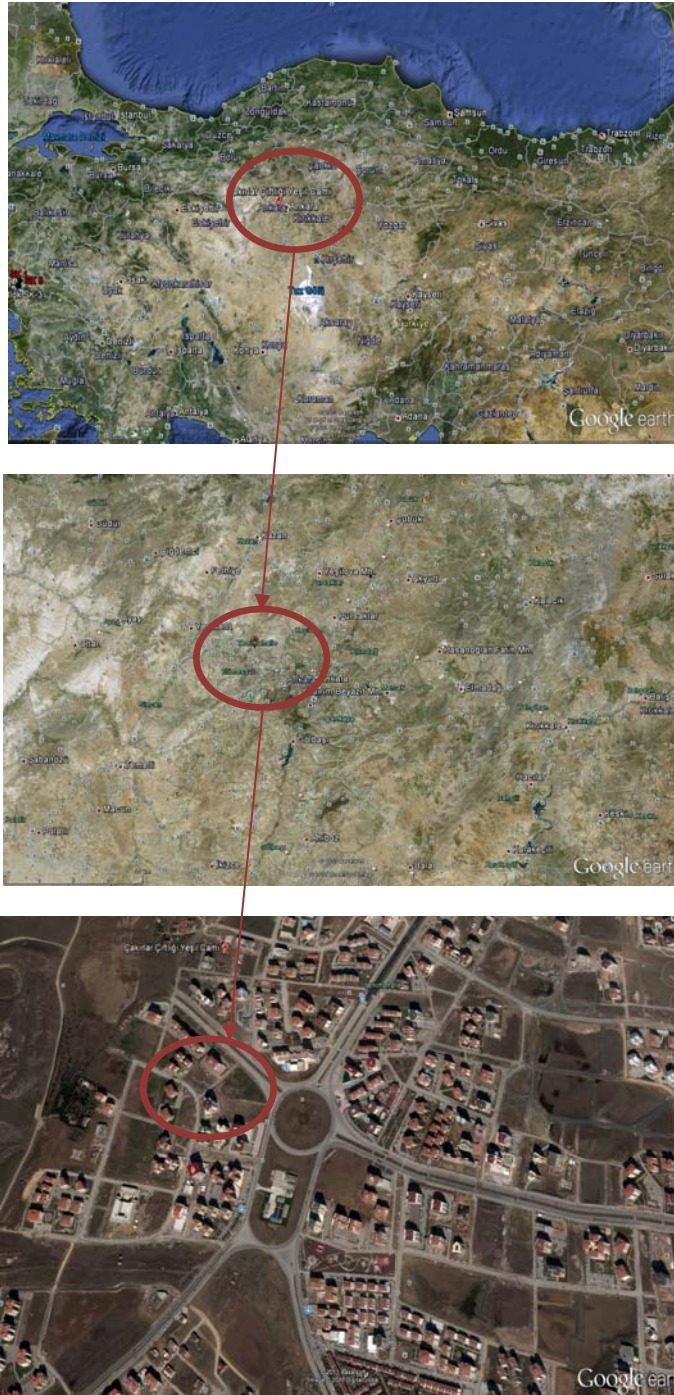
## LIST OF NOTATIONS USED IN THE TEXT

$A_1$ and $A_2$ :	elastic settlement factors to be taken from Figure 2.12
$A_g$ :	cross sectional area of column
$A_{\text{foundation}}$ :	Area of foundation
$A_{\text{column}}$ :	Area of the rammed stone columns
$A_{\text{shaft}}$ :	area of the column shaft
$B$ :	footing width
$B_p$ :	width of square loading plate
$B_{fs}$ :	width of full-size footing
$c_u$ :	undrained cohesion of soil
$c_{u,g}$ :	undrained cohesion of rammed stone column
$c$ :	cohesion of soil
$c_{\text{comp}}$ :	composite cohesion
$c'$ :	effective cohesion of soil
$c'_g$ :	effective cohesion of the rammed aggregate material
$c_1$ :	slope of the straight line
$c_2$ :	y-axis intercept of the straight line
$d_{\text{shaft}}$ :	actual shaft diameter of the column after damping
$d$ :	nominal diameter of the constructed column
$D_e$ :	effective diameter of the column
$d_f$ :	depth of footing
$e_0$ :	initial void ratio
$\epsilon_g$ :	axial strain of the rammed stone column
$E$ :	Elastic modulus of the soil
$E_s$ :	modulus of elasticity of the matrix soil
$E_{\text{oed}}$ :	oedometer modulus of the soil
$E_g$ :	elastic modulus of rammed stone column
$E_{\text{oed,g}}$ :	oedometer modulus of rammed stone column material
$F_v$ :	vertical force
$F'_c, F'_q$ :	cavity expansion factors
$f_s$ :	average unit friction along the shaft
$H_{lz}$ :	lower zone layer thickness
$H_{uz}$ :	upper zone layer thickness
$H_{\text{shaft}}$ :	Shaft length of the rammed stone column
$H_0$ :	nominal length of column
$I_r$ :	rigidity index
$I_q$ :	Westergaard effect factor
$K_p$ :	Rankine passive earth pressure coefficient
$K_{p,g}$ :	passive earth pressure coefficient of the rammed stone column
$k$ :	stiffness
$k_g$ :	Subgrade modulus of rammed stone columns
$k_s$ :	stiffness of the soil matrix
$k_{mp}$ :	modulus of subgrade reaction determined from square plate load test
$k_m$ :	modulus of subgrade reaction of full-scale footing
$L$ :	footing length
$L_g$ :	Length of rammed stone columns
$n$ :	stress concentration ratio
$N_c, N_q$ and $N_\gamma$ :	bearing capacity factors
$P$ :	applied load
$p_{\text{avg,g}}$ :	average measured load in the pier
$q$ :	average normal stress at calculated depth where bulging failure is thought to

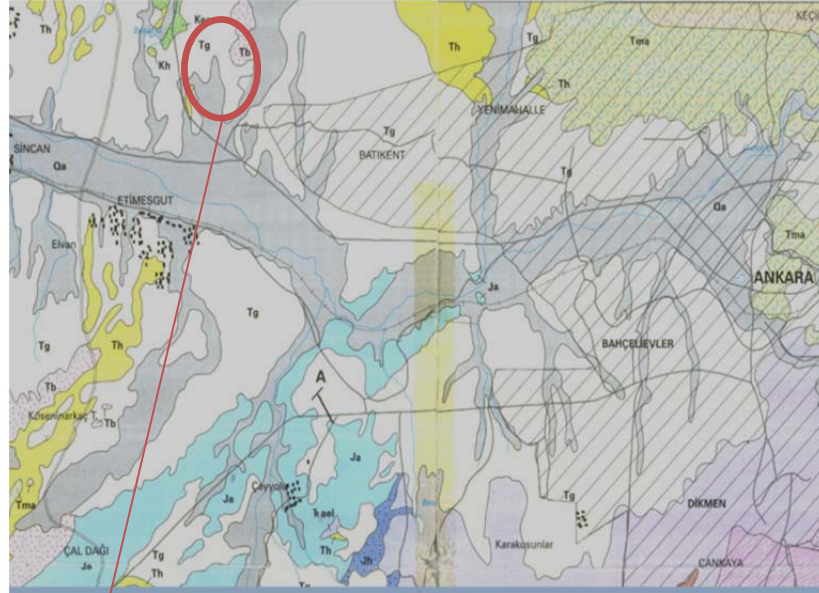
	occur
$\bar{q}$ :	effective overburden stress at the bearing elevation outside the footprint of the footing
$q_{tip}$ :	stress resisted at tip of the column
$q_{bottom}$ :	Ultimate bearing pressure at the bottom of reinforced soil
$q_{ult}$ :	ultimate bearing pressure
$q_o$ :	average applied stress
$q_g$ :	top of column stress
$q_s$ :	top of soil stress
$Q_{top}$ :	total load applied to the top of column
$Q_{shaft}$ :	shaft friction
$Q_{tip}$ :	end bearing of column
$Q_u$ :	estimated ultimate load
$R_a$ :	area replacement ratio
$R'_a$ :	area replacement ratio which is calculated by multiplying by reduction factor of 0.40
$s_c$ and $s_v$ :	shape factors
$s$ :	settlement
$s_g$ :	Center to center spacing between columns
$s_{uz}$ :	upper zone settlement
$s_{lz}$ :	lower zone settlement
$s_{i,uz}$ :	immediate settlement of the upper zone
$s_{i,lz}$ :	immediate settlement of the lower zone
$s_{c,lz}$ :	settlement from primary consolidation of the lower zone
$s_{s,lz}$ :	settlement from secondary consolidation of the lower zone
$s_{m,lz}$ :	settlement from changes in moisture within the lower zone
$s_g$ :	spacing of individual columns
$\nu$ :	Poisson's ratio
$z_b$ :	depth at which bulging occurs
$\emptyset_g$ :	internal friction angle of the rammed stone column aggregate material
$\emptyset'_g$ :	effective internal friction angle of the rammed stone column aggregate material
$\emptyset_s$ :	internal friction angle of the soil
$\emptyset'_s$ :	effective internal friction angle of the soil
$\emptyset_{comp}$ :	composite internal friction angle
$\gamma'_g$ :	dry unit weight of rammed stone column
$\gamma_g$ :	wet unit weight of the rammed stone column
$\gamma'_s$ :	dry unit weight of the soil
$\gamma_s$ :	wet unit weight of the soil
$\gamma'_w$ :	wet unit weight of the soil
$\gamma_s$ :	unit weight of soil
$\sigma_{ro}$ :	total radial stress
$\sigma'_{vo}$ :	initial vertical effective stress
$\sigma_{r,lim}$ :	limit radial stress
$\sigma_1$ :	ultimate vertical stress
$\sigma_3$ :	limiting radial stress
$\sigma_g$ :	effecting vertical stress on the column
$\sigma_c$ :	effecting vertical stress on the cohesive soil
$\sigma^{v,avg}$ :	effective vertical stress at midpoint of the shaft length
$\sigma'_{v,tip}$ :	overburden stress at the elevation of the tip of the column
$u_0$ :	pore water pressure
$\Delta_q$ :	stress increment
$\Delta_{Lt}$ :	measured shortening length of the column at each loading step
$\delta$ :	displacement

## APPENDIX A

The general database consisting of laboratory and in-situ test obtained from the current site soils in this study are given in Appendix A. (refer to Chapter 3).



Location map of the site



	Oa Alluvium; sand, gravel		R <sub>ak</sub> Keçikaya formation; grey, white coloured limestone
	Tg Gölbaşı formation; conglomerate, sandstone, mudstone		R <sub>ao</sub> Ortaköy formation; spilite, diabase, tuff, volcanogenic sandstone, agglomerate
	Tt Tekke volcanics; andesite, trachyandesite, tuff, agglomerate		R <sub>am</sub> İmrahor limestone member; limestone having original relationship with volcanics
	Tma Mamak formation; agglomerate, tuff, andesite		R <sub>ael</sub> Elmadğ formation; metaconglomerate, metasandstone, sandy limestone, sandstone, limestone, volcanogenic sandstone, agglomerate
	Th Haçlıli formation; sandstone, siltstone, marl, clayey limestone, tuff, gypsum, bituminous shale		R <sub>em</sub> Emr formation; muscovite-quartz schist, serisite-chlorite-quartz schist, serisite-chlorite schist, fillite, calcschist, metavolcanics, metaconglomerate

Geological map of the site

Standard penetration test	
Project name:	Thesis
Location:	Çakırlar Çiftliği, Yenimahalle, Ankara
Machine Type	Rotary, D-500
Groundwater level	-

Borehole no	Depth	SPT 15	SPT 30	SPT 45	SPT N # of blows	Soil definition
BH-1	1.50-1.95	4	5	4	9	Brown sandy silty clay
	3.30-3.75	4	5	5	10	
	4.50-4.95	7	7	5	12	
	6.30-6.75	5	4	6	10	
	7.50-7.95	7	8	7	15	
	9.55-10.00	10	12	7	19	
	10.50-10.95	18	20	12	32	
	12.25-12.70	15	20	25	45	
	13.50-13.95	18	20	29	49	
	15.00-15.45	28	35	30	50 +	
BH-2	1.50-1.95	2	3	3	6	Brown sandy silty clay
	3.00-3.45	3	3	6	9	
	4.50-4.95	4	4	4	8	
	6.35-6.80	5	4	9	13	
	7.50-7.95	7	9	8	17	
	9.45-9.90	7	10	9	19	
	10.50-10.95	10	13	25	38	
	12.35-12.80	20	25	21	46	
	13.50-13.95	25	30	25	50+	
	15.00-15.45	20	35	30	50 +	
BH-3	1.50-1.95	4	4	6	10	Light brown sandy silty clay
	3.00-3.45	4	3	4	7	
	4.50-4.95	5	5	6	11	
	6.50-6.95	6	7	7	14	
	7.50-7.95	12	15	6	21	
	9.00-9.45	10	10	12	22	
	10.50-10.95	22	25	16	41	
	12.00-12.45	22	25	24	49	
	13.50-13.95	30	33	35	50+	
	15.00-15.45	20	25	35	50 +	

Laboratory test results of subsoil					
Borehole number	Depth of sample (m)	Triaxial shear tests (UU)		Direct shear tests (CD)	
		$c_u$ (kPa)	$\phi$ (°)	$c'$ (kPa)	$\phi'$ (°)
BH-1	3.00-3.30	43	7		
BH-1	9.00-9.55			5.69	23.6
BH-2	2.50-3.00			6.904	33.8
BH-2	6.00-6.35	53.03	3		
BH-2	9.00-9.45			9	13.80
BH-3	2.50-3.00	48.54	8		
BH-3	6.00-6.50			10.36	29.1
BH-3	11.00-11.50	94.17	12		

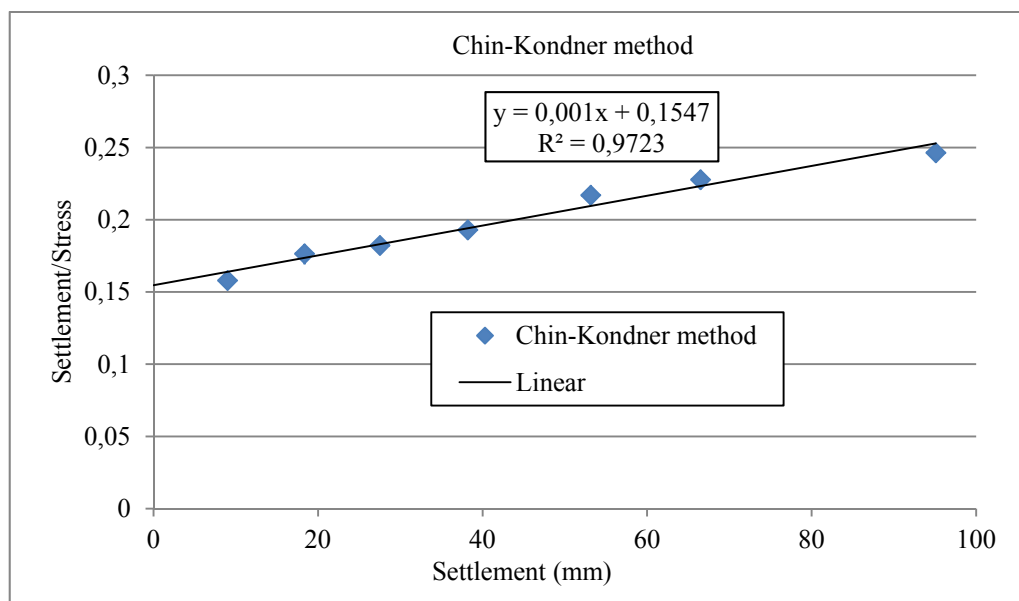
Laboratory test results of subsoil							
Borehole No.	Depth (m)	No:4 retainig (%)	No:200 passing (%)	LL (%)	PL (%)	PI (%)	USCS
BH-1	1.50-1.95	0	65.8	39	25	14	CL
	3.00-3.30	9.2	71.2	62	26	36	CH
	6.30-6.75	1.8	89.9	65	31	34	CH
	9.00-9.55	-					
	15.00-15.45	-					
BH-2	1.50-1.95	4.58	74.65	49	25	24	CL
	4.50-4.95	0	80	46	23	23	CL
	6.00-6.35	0	89	70	32	38	CH
	9.00-9.45	0.9	83.2	68	26	42	CH
BH-3	1.50-1.95	0	96.79	38	18	20	CL
	2.50-3.00	0	89.23	42	22	21	CL
	6.00-6.50	3.97	65.48	46	24	22	CL
	7.50-7.95	2.3	86.3	76	34	42	CH
	15.00-15.45						

Laboratory test results of subsoil							
Borehole No	Test depth (m)	Limit pressure, $P_1$ (kg/cm <sup>2</sup> )	Initial pressure, $P_i$ (kg/cm <sup>2</sup> )	Final pressure, $P_f$ (kg/cm <sup>2</sup> )	Menard's modulus, $E_m$ (kg/cm <sup>2</sup> )	Menard's $\alpha$ factor	Oedemeter modulus, $E_{oed}$ (kg/cm <sup>2</sup> )
BH-1	2	3.8	0.4	2.2	42	0.67	62.68
	4	3.9	0.4	1.7	40	0.67	59.70
	6	2.8	0.4	1.6	24	0.67	35.82
	8	2.7	0.4	1.7	27	0.67	40.30
	10	2.6	0.4	1.6	22	0.67	32.84
BH-2	2	4.0	0.8	2.2	45	0.67	67.16
	4	3.7	0.4	2.1	35	0.67	52.24
	6	2.8	0.4	1.6	28	0.67	41.79
	8	2.4	0.4	1.6	25	0.67	37.31
	10	2.8	0.8	2	29	0.67	43.28
	12	2.9	0.8	2	22	0.67	32.84

## **APPENDIX B**

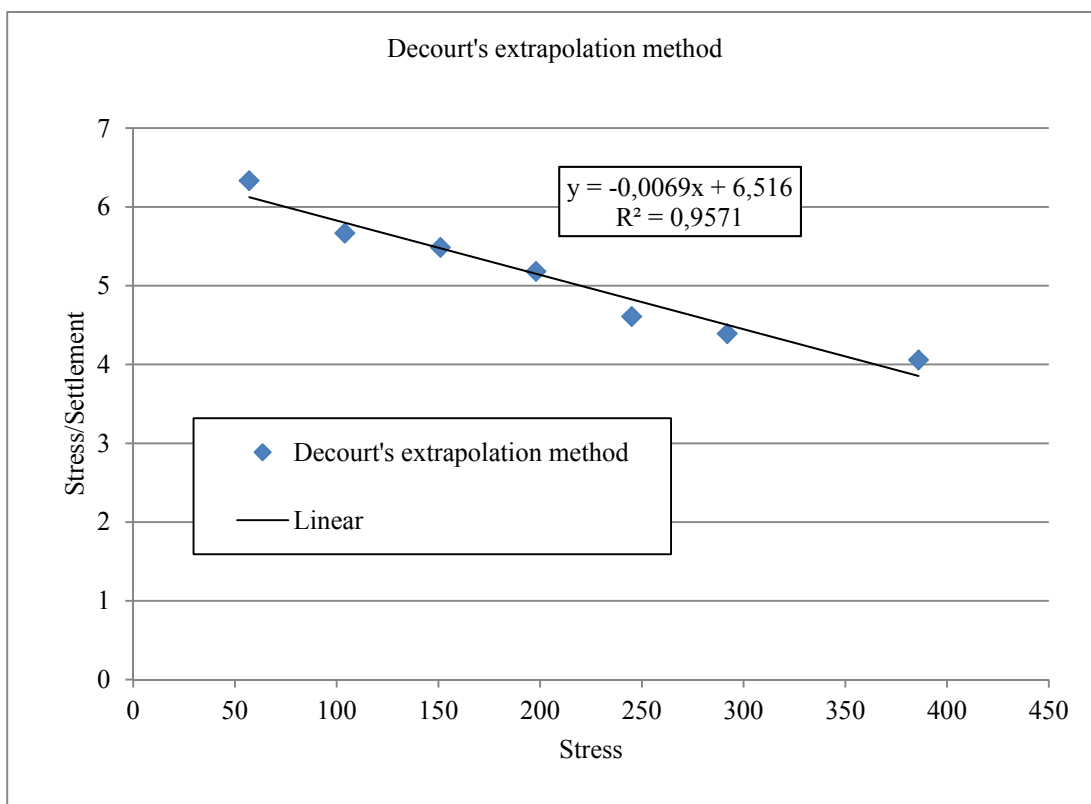
Ultimate bearing capacity calculations of a rammed stone column reinforced soil which is estimated using different methods applied to stress-settlement data obtained from the plate load test on the specific site in this study are given in Appendix B (refer to Chapter 3).

Ultimate bearing capacity estimation from Chin-Kondner method		
Applied stress, q (kPa)	Measured settlement, s (mm)	$s/q$
0	0	-
57	9	0.157895
104	18.35	0.176442
151	27.52	0.182252
198	38.21	0.19298
245	53.16	0,21698
292	66.5	0.22774
386	95.1	0.246373



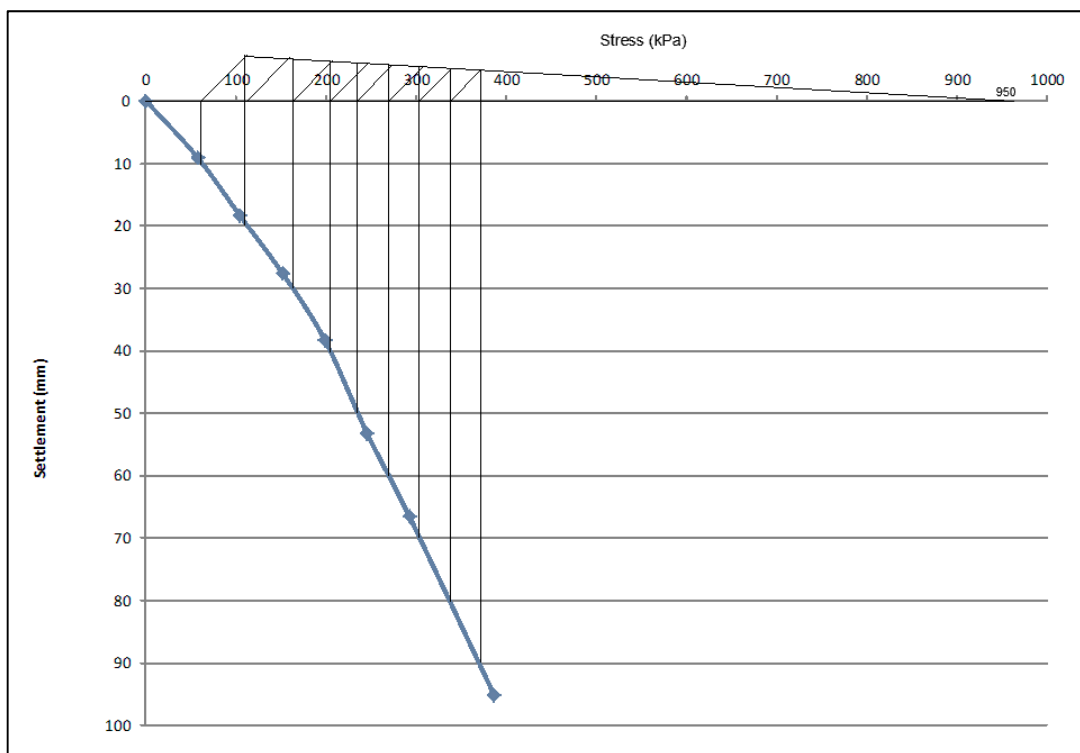
$$Q_{ult} = \frac{1}{c_1} = \frac{1}{0.001} = 1000 \text{ kPa}$$

Ultimate bearing capacity estimation from Decourt's extrapolation method		
Applied stress, q (kPa)	Measured settlement, s (mm)	$q/s$
0	0	-
57	9	6.333333
104	18.35	5.667575
151	27.52	5.486919
198	38.21	5.18189
245	53.16	4.608728
292	66.5	4.390977
386	95.1	4.058885



$$Q_{ult.} = \frac{c_2}{c_1} = \frac{6.516}{0.0069} = 944 \text{ kPa}$$

Ultimate bearing capacity estimation from Mazurkiewicz's method	
Applied stress, q (kPa)	Measured settlement, s (mm)
0	0
57	9
104	18.35
151	27.52
198	38.21
245	53.16
292	66.5
386	95.1

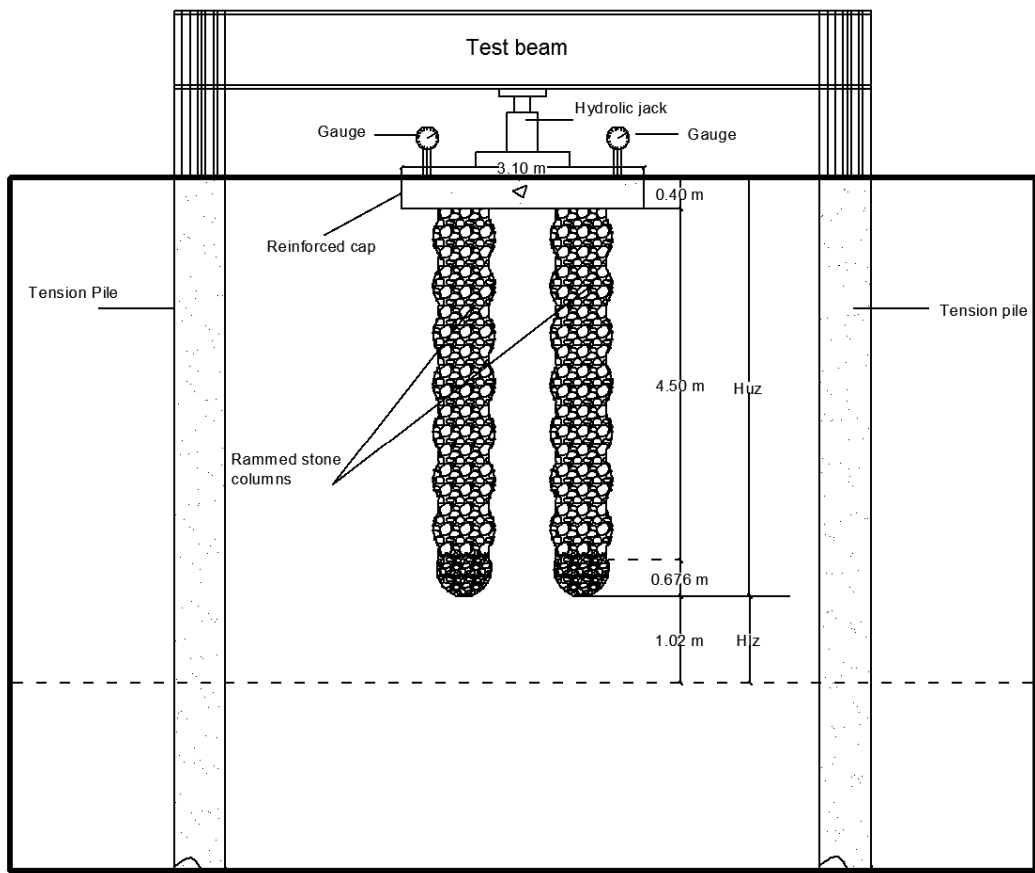


The extent of the line which goes through the intersections of vertical lines and 45° inclined lines indicates a maximum capacity of 950 kPa as shown in Figure 3.16.

$$Q_{ult.} = 950 \text{ kPa}$$

## **APPENDIX C**

Some pictures during the plate load test on a single rammed stone column and a group of rammed stone columns in this study are given in Appendix C (refer to Chapter 3).



Conducted plate load test setup on reinforced soil



A view of the load test on a group of rammed stone columns



A view of the load test on a single rammed stone column



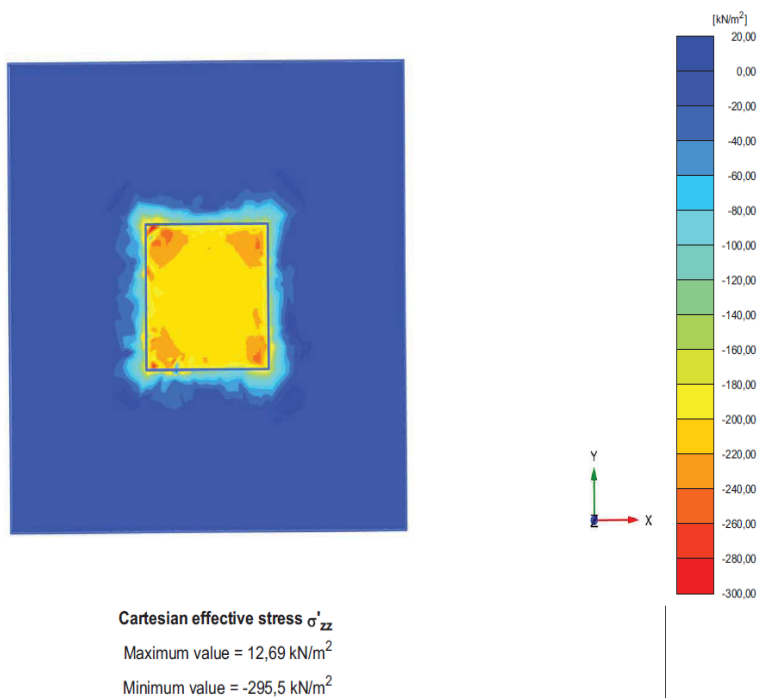
A view of the study area during settlement records of the plate load test



Diameter measurement of a constructed rammed stone column



Appearance of the constructed rammed stone column after excavation of the surrounding soil



Stresses acting on reinforced soil